CHALMERS
UNIVERSITY OF TECHNOLOGY

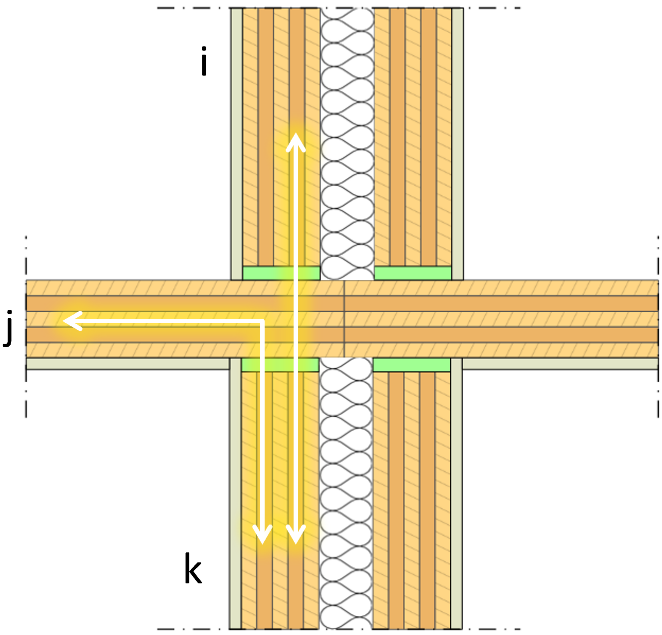

Acoustic performance of junctions in cross laminated timber constructions

Master's thesis in the Master's Programme Sound and Vibration

JESPER HÖRNMARK

Department of Architecture and Civil Engineering
Chalmers University of Technology
Gothenburg, Sweden 2019

Master's thesis ACEX60-19-1

Acoustic performance of junctions in cross laminated timber constructions

JESPER HÖRNMARK

Department of Architecture and Civil Engineering
Division of Applied Acoustics
Chalmers University of Technology
Gothenburg, Sweden 2019

Acoustic performance of junctions in cross laminated timber constructions
JESPER HÖRNMARK

Supervisor: Klas Hagberg
Examiner: Jens Forssén

Master's Thesis ACEX60-19-1
Department of Architecture and Civil Engineering
Division of Applied Acoustics
Chalmers University of Technology
SE-412 96 Gothenburg
Telephone +46 31 772 1000

Cover: Cross laminated timber X-junction.

Acoustic performance of junctions in cross laminated timber constructions
JESPER HÖRNMARK
Department of Architecture and Civil Engineering
Chalmers University of Technology

Abstract

With the emergence of cross laminated timber (CLT) as a structural material on the global market, the need to understand the acoustical behavior of buildings constructed with the material grows. CLT faces a set of challenges that concrete or masonry do not; being low density, high in stiffness, sometimes isotropic and sometimes orthotropic depending on the composition. Flanking sound transmission often becomes an issue in the acoustic performance of mass timber buildings. While direct sound transmission can be treated with conventional methods e.g. additional layers, the flanking paths are more complicated to treat since they need to transfer loads over the length of the element. This master's thesis aims to investigate the flanking paths in cross laminated timber buildings by measuring the structure-borne vibration reduction index (K_{ij}) in realized buildings. The in-field measurements are compared to standardized estimation models and lab measurements published in past research.

This thesis finds that standardized estimations underestimate the performance of the examined junctions in low frequencies. The lab measurements are closer to the in-field performance but exaggerate the influence of metal connections and mass-spring behavior of junctions with elastic interlayers. Additionally the theory and results indicates that external loads on the junction play a major role in the resulting performance. Elastic interlayers are not as effective in low levels as in the high levels of any given building, presenting a challenge as mass timber structures are increasingly being built taller.

Acknowledgements

This thesis is the result of two years of master's studies at the Division of Applied Acoustics at the Department of Civil and Environmental Engineering of Chalmers University of Technology. It had not been possible without the support of the Acoustic group at WSP Malmö, my supervisor Klas Hagberg at Acouwood and my examiner Jens Forssén at Chalmers. Thank you!

I also want to thank Natalie and my family for their unfailing support during my time in school.

Keywords: cross laminated timber, CLT, mass timber, vibration reduction index, Kij, flanking transmission.

Contents

List of Figures

List of Tables

List of symbols and notations

a	Absorption length [m]
B	Bending stiffness [Nm]
B_{eff}	Effective bending stiffness [Nm]
CLT	Cross laminated timber
c_B	Phase velocity [m/s]
c_g	Group velocity [m/s]
c_L	Longitudinal wave speed [m/s]
c_T	Transverse wave speed [m/s]
c_0	Speed of sound in air [m/s]
$D_{v,ij}$	Average surface velocity level difference [m/s]
$\bar{D}_{v,ij}$	Direction averaged surface velocity level difference [m/s]
E	Young's modulus [N/m^2]
f	Frequency [Hz]
f_c	Critical frequency [Hz]
FEM	Finite element model
G	Shear modulus [N/m^2]
k_B	Bending wave number
K_{ij}	Vibration reduction index [dB]
$l_{i,j}$	Junction length [m]
m	Mass [kg]
m'	Mass per unit length [kg/m]
m"	Mass per unit area [kg/m^2]
MOF	Modal overlap factor
n$_B$	Bending wave modal density
N(k)	Number of modes
R	Reduction index [dB]
S	Surface of plate [m^2]
T_S	Structural reverberation time [s]
v	Velocity [m/s]
Y_{mob}	Mobility [m/Ns]
λ	Wave length [m]
ν	Poisson's ratio [-]
ρ	Density [kg/m^3]
ρ	Reflection coefficient [-]
σ	Radiation efficiency [-]
τ	Transmission coefficient [-]
ψ	Mode shape
ω	Angular frequency

1 Background

Cross laminated timber is increasingly making timber a viable alternative again as a load-bearing structural material for new constructions around the world; a market dominated by steel and concrete since the beginning of the 20th century (Brandner, Flatscher, Ringhofer, Schickhofer, and Thiel, 2016). The main factors why CLT is gaining traction include but are not limited to (Barber, 2015) (Darby, Elmualim, and Kelly, 2013):

1. Low carbon footprint
2. Fire resistance
3. Load-bearing in- and out-of-plane
4. Lightweight
5. Prefabricated modules allowing easy and accurate assembly

One study found that the worldwide production volume has increased from 500 000 m^3/a in 2012 to 625 000 m^3/a in 2014 and thereafter was expected to grow to 700 000 m^3/a in 2017 (Brandner, Flatscher, Ringhofer, Schickhofer, and Thiel, 2016). Currently in Sweden the sole production facility of CLT, run by Martinson, increased its production capacity from 7000 m^3/a to 22 000 m^3/a in 2017 (Aronsson, 2017b). In 2019, Stora Enso's new CLT production facility is set to open with a capacity of producing 100 000 m^3 annually (Aronsson, 2017a).

In virtually all of Europe wooden structures higher than two stories were banned until the 1990's (Östman and Källsner, 2011). In Sweden the ban was lifted in 1994 (Hansson and Hervén, 2011). There has been several showcases of CLT's capability as a high-rise building material since then. "Treet (the tree)" in Bergen, Norway famously became the worlds tallest timber building in 2015 at 14 stories (Abrahamsen, 2015). The student residence at the University of British Columbia overtook the title in 2017 with 18 stories (Gintoff, 2016). This high-rise building race is crucial for CLT to prove its value and become a serious contender to concrete and steel on the global market. As CLT gains traction as a building material for high-rise constructions, the need for empirical data concerning acoustics in these types of constructions increases.

1.1 Composition

Cross laminated timber elements consists of layers. One sheet of lamellas is glued to another sheet rotated perpendicular to the fibers of the first sheet. This continues for every layer added (Figure 1.1). CLT elements are always made up of an uneven number of layers. Most commonly ranging from 3 to 7 layers.

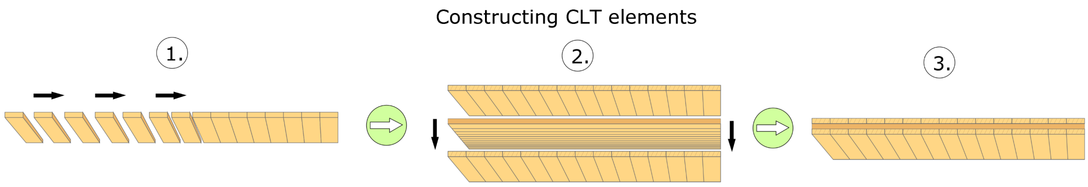

Figure 1.1: CLT element assembly

Because the element structure has fibers going in both directions of the plate it becomes load-bearing in all directions. This can be compared to glulam which is load-bearing in one direction, since all fibers are parallel to each other (Figure 1.2). This means the material can compete with other materials, such as concrete. Though not as strong in compression, it is more lightweight and therefore does not need to carry as big of a load.

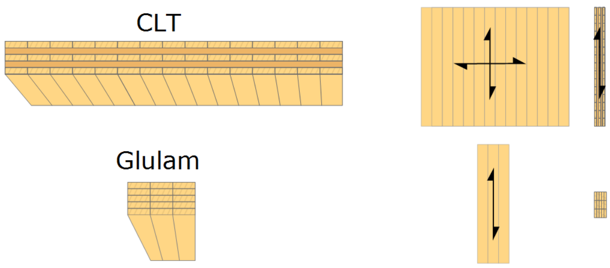

Figure 1.2: load-bearing capabilities of CLT vs glulam

1.2 Environmental impact

If the life cycle assessment of the same multi-story building constructed with a concrete frame and a CLT construction is compared, then the ecological benefits of mass timber becomes clear. If the timber is sourced from sustainably managed forests, the E_c (embodied carbon) ranged from -1021tCO2e for re-use to +126tCO2e for incineration without energy recovery as the end of life treatment. That is 1525tCO2e and 378tCO2e less than that of the concrete building respectively (Darby, Elmualim, and Kelly, 2013). This is partly because the timber stores CO_2 even as it is functioning as a building material.

With increasing national and international sustainability goals combined with the fact that CLT can measure up in strength leads to the conclusion that high-rise CLT constructions are here to stay.

1.3 Fire safety

Conventional wisdom tells us that wooden structures are a fire hazard and is the reason high-rise timber constructions have been restricted until recently (Östman and Källsner, 2011). However, the wooden structures of old were often constructed with timber pillars, beams, and single layer wooden walls; unlike the mass-timber systems that are currently being used for new timber structures. Just like any other combustible material, CLT has the potential to feed a fire. The difference is that during fire-exposure, massive timber products generate a thick layer of low-density insulating char on the element side exposed to the fire and thereby protects the timber behind from elevated heat effects (Dagenais, White, and Sumathipala, 2013). When done right, this would ensure structural integrity for a longer period of time than steel (Barber, 2015). How well the CLT structure performs does however depend on a couple of factors, e.g. type of adhesive, panel thickness, laminate thickness, wood species, panel-to-panel joint configuration, etc.(Dagenais, White, and Sumathipala, 2013).

1.4 Health benefits

It has been proven that exposure to nature reduces stress and blood pressure levels as well as promote creativity and concentration. New findings suggest that exposure to wooden surfaces indoors will lead to similar benefits.The study "Wood and human health" had students perform different tasks in rooms with and without exposed wooden surfaces. The stress level, as measured by sympathetic nervous system activation, was lower in the room with exposed wood (Fell, 2013).

1.5 Previous measurements

Rothoblaas, "Flanksound project"
Italian CLT-solutions producer funded a research project called "The flanksound project". Like the title hints at, the goal was to figure out flanking transmission in CLT structures i.e. measuring the vibration reduction indexes "K_{ij}". It was a controlled lab experiment of different junction compositions consisting of two to four elements depending on the junction. The CLT-elements came from seven different manufacturers. The experiment focused on the influence of screws, brackets and interlayers.

Timpte, "Vibration Reduction Indices of Cross Laminated Timber Structures", 2016
This master thesis gathered vibration reduction indexes from eight different institutes and compared the different junctions. The focus was similar to that of the Flanksound project, to see how changing different properties of the junction changes the overall flanking performance of the structure. The measurement data provided is mainly from lab.

Bard, Davidsson and Wernberg, "Sound and vibrations investigations in a multi-family wooden frame building", 2010
This paper measured impact noise transmission in a CLT-building. The measured paths were direct, first and second order flanking. The main focus was to determine the noise isolation performance difference between upper and lower levels in the building.

2
Aim

The purpose of this paper is to shed light on how well a CLT construction performs acoustically (especially in mid to high-rise buildings). The focus is on determining the transmission through joints, causing flanking between rooms. This is measured in realized buildings, and compared to previous research and theory.

Goals:

1. Perform vibration analysis of CLT elements
2. Gather vibration reduction indexes measured in lab, currently available in published studies
3. Perform similar measurements in-field according to ISO 10848-1
4. Calculate corresponding vibration reduction indexes as described in ISO 12354
5. Compare the three sources of junction transmission data

3

Vibration analysis of CLT elements

The material properties of CLT, being both stiff and low density, leads to issues regarding sound insulation (Santoni, Fausti, Schoenwald, and Tröbs, 2016a). In Figure 3.1 a product from Italian CLT-solutions producer Rothoblaas is shown. It is a simple CLT wall element with an elastic layer and plasterboard. The related sound reduction index graph shows that there is a clear area in the frequency range between 200-800 Hz where the element is under performing. This tends to be an issue for most CLT elements without excessive amounts of external layers.

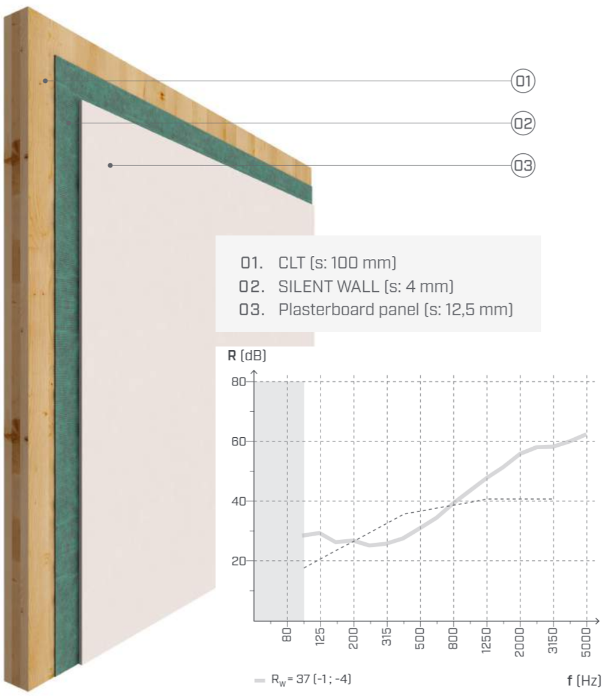

Figure 3.1: CLT wall element example
Credit: Rothoblaas soundproofing solutions (Rothoblaas, 2018)

3.1 Modal analysis

The degree to which cross laminated timber is orthotropic depends on its layered composition. A 3-layered composition with identical layers will have very different cross sections depending on the angle the element is cut. One direction will be stiff in two thirds of the cross section area, this will be called the "major direction". The other direction will be stiff in one third of the cross section's area, this will be referred to as the "minor direction". Adding more layers or compensating with thicker layers in the minor direction will make the element more akin to that of an isotropic material. In the following section a 3-ply plate with identical layers is used. This is a relatively common element composition which is rather orthotropic in its nature which will showcase the potential challenges specific to CLT.

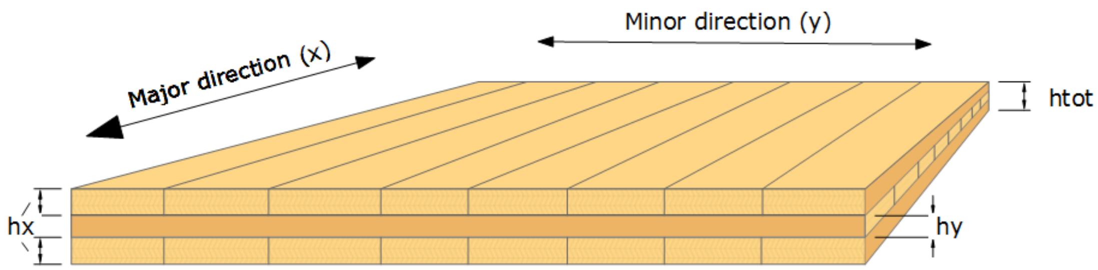

Figure 3.2: CLT element strength directions

Table 3.1 details the stiffness of a number of compositions according to the structural material property sheet of a manufacturer of CLT (Martinsons). According to the sheet, two different strength classes of timber are used for the two principal directions of one element. Strength class C14 is used for the minor or "weak" direction. This class allows for branches 1/2 the width of the lamella and the whole thickness. It is traditionally used as load-bearing wall studs where requirements on deformations are low. The major or "strong" direction is made up of timber of the strength class C24. This class allows for branches 1/4 of the thickness of the lamella and 1/2 of the thickness. Timber made out of this strength class is primarily used as structural elements which require low deformation, such as trusses and load-bearing floors. This means that not only is there a potential difference in the ratio of the area of fibers perpendicular to the total area of the cross section of any given direction, but the strength class of the stiff lamellas are different between the two cross sections as well. This means that a CLT element is potentially highly orthotropic or relatively isotropic depending on the composition.

Thickness (mm) - layers	Major (MPa)	Minor (MPa)
80 - 3ply	10832	474
100 - 3ply	10311	794
100 - 5ply*	8760	1749
150 - 5ply	8760	1749
170 - 7ply	6877	2908
210 - 7ply	7891	2284

Table 3.1: CLT element properties
*Strength class C24 in major and minor direction

Since a lot of the theoretical models for vibration analysis assume homogeneous isotropic material properties, the major and minor direction will be utilized in the following equations to showcase worst and best case scenarios. The idea is that the true behavior is a combination of the two. The phase velocity is dependent on the stiffness of the material which in turn is different for different directions of the plate as discussed above. The bending wave number-spectrum can therefore be calculated in the major and minor direction and the two spectrums are then combined into one. The calculations will depend on the angle "θ", that is the angle relative to the fiber direction of the outer stiff layer as described in Figure 3.3. The angles range from 0 to $\pi/2$ since all other angles are redundant information (Santoni, Schoenwald, Van Damme, Tröbs, and Fausti, 2016b). The element analyzed will have the dimensions 100(mm)-3ply (Table 3.1) with the length L_x=2.9m and L_y=4.2m to emulate a wall, where X is the major direction and Y the minor.

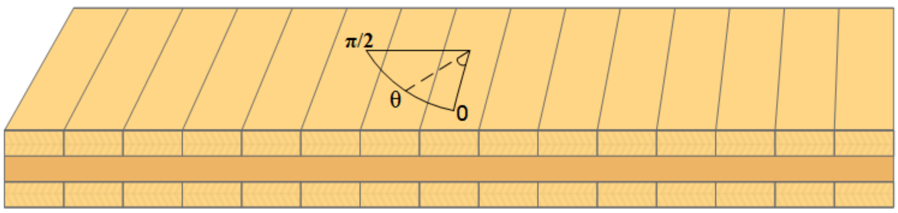

Figure 3.3: Wave propogation angle

The wave number is calculated for the different angles as (Santoni, Schoenwald, Van Damme, Tröbs, and Fausti, 2016b)

$$k_B(\omega,\theta) = \sqrt{(k_{B,x}\cos\theta)^2 + (k_{B,y}\sin\theta)^2} \tag{3.1}$$

where

$$k_{B,i} = \sqrt[4]{\frac{\rho m'\omega^2}{B_i}}\left(1 + \frac{j\eta}{4}\right) \tag{3.2}$$

and the bending stiffness is related to the major and minor direction as

$$B_i = \frac{E_i h^3}{12(1-\nu_i^2)} \tag{3.3}$$

The literature available provides very different values for damping ranging from 0.5 to 0.2. There are studies suggesting that the damping decrease with frequency(Santoni, Schoenwald, Van Damme, Tröbs, and Fausti, 2016b). Since this analysis's main focus is low to mid frequencies, a static loss factor of 0.08 will be used for all frequencies. The Poisson's ratios are high for timber and the ones used in this analysis are ν_x=0.44, ν_y=0.64 and $\nu_{xy} = \sqrt{\nu_x \nu_y}$ (Augustsson, 2016).

To get a better understanding of the behavior of CLT, a modal analysis can be done for the CLT-plate. The mode shapes can be plotted according to (Hopkins, 2007)

$$\psi_{p,q} = sin\Big(\frac{p\pi X}{L_x}\Big) sin\Big(\frac{q\pi Y}{L_y}\Big) \tag{3.4}$$

and the related natural frequencies can for an orthotropic plate be calculated as

$$f_{p,q} = \frac{\pi h}{2\sqrt{12}} \left(c_{L,x} \left(\frac{p}{L_x}\right)^2 + c_{L,y} \left(\frac{q}{L_y}\right)^2 \right) \tag{3.5}$$

for the isotropic case

$$f_{p,q} = \frac{\pi h c_{L,i}}{4\sqrt{3}} \left(\left(\frac{p}{L_x}\right)^2 + \left(\frac{q}{L_y}\right)^2 \right) \tag{3.6}$$

where p and q are a set of integers and $c_{L,i}$ is the longitudinal wave speed for the major and minor direction

$$c_{L,i} = \sqrt{\frac{E_i}{\rho(1-\nu_i^2)}} \tag{3.7}$$

The mode shapes and their corresponding frequencies are shown in Figure 5.2. The frequency in black is the orthotropic eigenvalue.

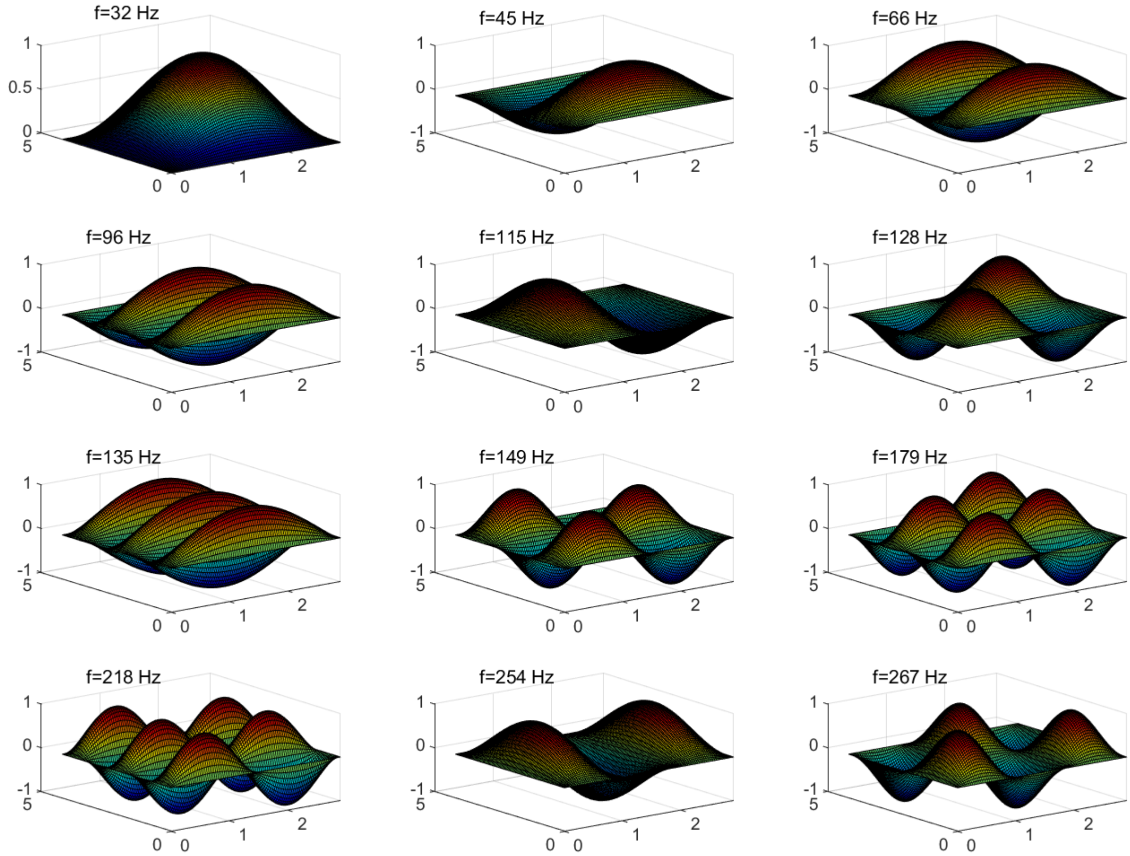

Figure 3.4: Mode shapes of 100-3ply 2.9m x 4.2m CLT plate

The number of bending wave modes below the wave number k can be calculated as

$$N(k_B) = \frac{k_B^2 S}{4\pi} \tag{3.8}$$

and plotted over frequency (Figure 3.5). The mode count is the number of modes within the specified bandwidth. In this case one-third octave bands.

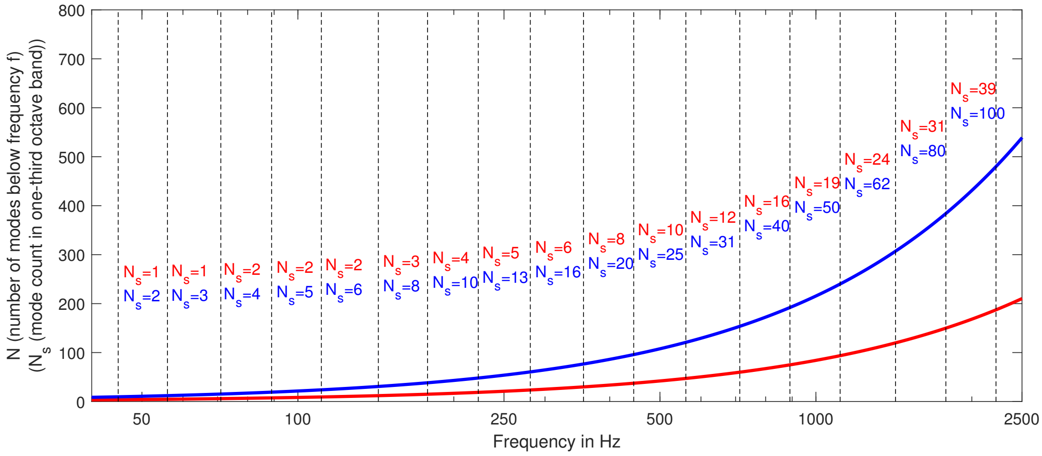

Figure 3.5: Number of modes below frequency f (lines). Mode count (text) red=major direction, blue=minor direction (100-3ply CLT plate)

The modal overlap factor M indicates how much overlap there is in the modal response. It is the ratio of the width of a 3 dB modal bandwidth to the width of the average frequency spacing between resonance peaks. This is highly dependent on the damping of the structure. Methods that rely on simplifications of the modal response such as SEA (statistical energy analysis) should only be used when the modal overlap factor is greater than one, since that frequency range provides more statistical certainty. The MOF for the studied plate can be seen in Figure 3.6.

$$M = \frac{\delta f_{3dB}}{\delta f} = f \eta n_B \tag{3.9}$$

where n is the modal density. The modal density for bending waves in the plate can be derived from the number of modes under the wave number k

$$n_B(f) = \frac{2\pi}{c_g} \frac{\delta N(k_B)}{\delta k_B} \tag{3.10}$$

where c_g is the group velocity of the plate, $c_g = 2c_B$.

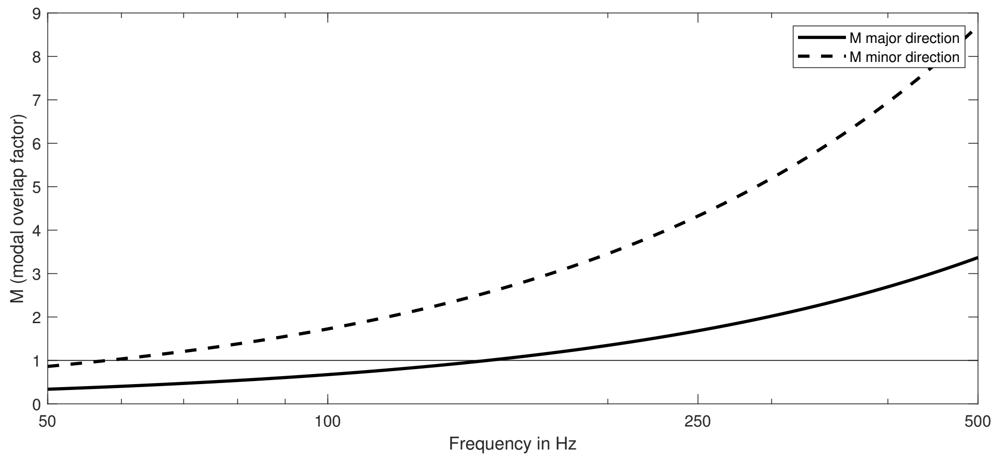

Figure 3.6: Modal overlap factor (MOF) (100-3ply CLT plate)

3.2 Vibration field

The velocity field of a plate can be studied in three dimensions. It can be estimated over frequency for a finite number of points on the plate for one excitation point as (Kropp, 2015)

$$v(x,y,\omega) = j\omega\frac{4}{\rho h L_x L_y}\sum_{p,q}\frac{F_0(\omega)\sin\left(\frac{p\pi x_0}{L_x}\right)\sin\left(\frac{q\pi y_0}{L_y}\right)\sin\left(\frac{p\pi x}{L_x}\right)\sin\left(\frac{q\pi y}{L_y}\right)}{\omega_{p,q}^2-\omega^2} \tag{3.11}$$

in order to include damping of the structure

$$v(x,y,\omega) = j\omega\frac{4}{\rho h L_x L_y}\sum_{p,q}\frac{F_0(\omega)\sin\left(\frac{p\pi x_0}{L_x}\right)\sin\left(\frac{q\pi y_0}{L_y}\right)\sin\left(\frac{p\pi x}{L_x}\right)\sin\left(\frac{q\pi y}{L_y}\right)}{\omega_{p,q}^2(1+j\eta)-\omega^2} \tag{3.12}$$

where F_0 is a point force acting in this case on position $x_0 = L_x/2, y_0 = L_y/2$ and

$$\omega_{p,q} = \sqrt{\frac{B_{eff}}{m''}}\left[\left(\frac{p\pi}{L_x}\right)^2+\left(\frac{q\pi}{L_y}\right)^2\right] \tag{3.13}$$

The equations are based on an isotropic model. Therefore it is necessary to find a way to treat the orthotropic element as isotropic. In literature it is sometimes suggested that orthotropic plates can be modelled as isotropic using the geometric average. However, it is not always clear when this is a valid assumption. The effective bending stiffness can then be estimated as (Hopkins, 2007)

$$B_{eff} = \sqrt{B_x B_y} \tag{3.14}$$

Figure 3.7 showcases the velocity of each individual mode as measured in the position $x = L_x/2, y = L_y/2$ which is the excitation point. It has been done for both an almost undamped case, $\eta = 0.001$ and a damped case, $\eta = 0.08$. It becomes clear that the more damped the structure is, the higher the modal overlap. As seen in Equation 3.12 the modes excited depend on where the point of excitation and measurement are. Despite there being more mode shapes of the plate, not all of them will be visible when looking at a single point of the plate or exciting it in only one position.

Figure 3.8 is the velocity at the driving point with the modes summed up as described in Equation 3.12. It can be compared to the driving point mobility of an infinite orthotropic plate that is calculated according to

$$Y_{mob,infinite\ plate} = \frac{1}{8\sqrt{B_{eff}m'}} \tag{3.15}$$

As the frequency and damping increase, the more the plate behaves like an infinite plate.

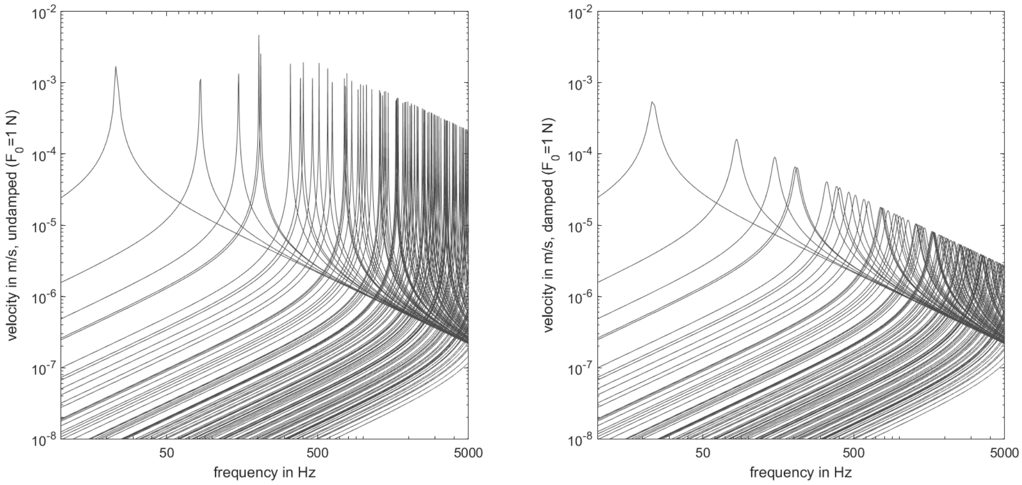

Figure 3.7: Driving point mobility per mode (100-3ply CLT plate)
Left: $\eta = 0.001$, Right:$\eta = 0.08$

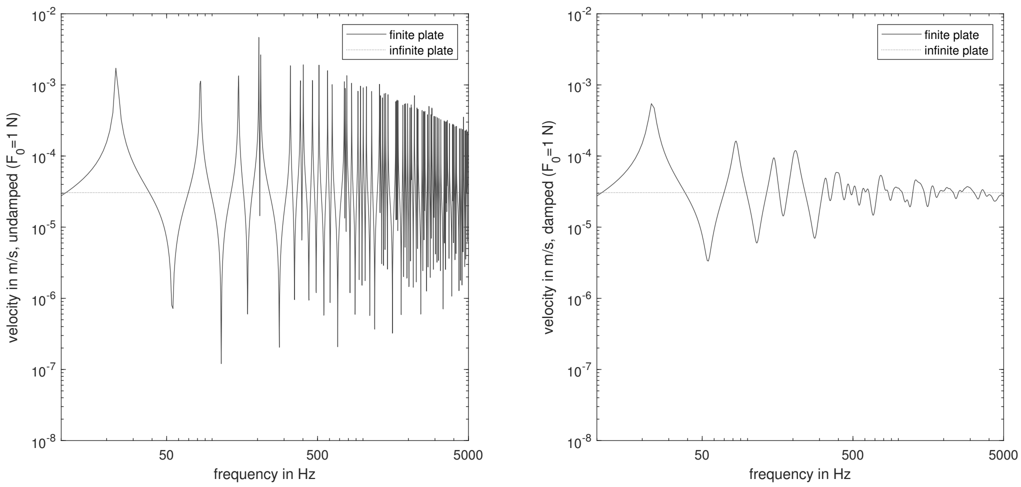

Figure 3.8: Driving point mobility x=L$_x/2, y = L_y/2(100 - 3plyCLTplate)$
$Left$:$\eta = 0.001$, Right:$\eta = 0.08$

Figure 3.9 showcase the difference to Figure 3.8 in modal response when keeping the same excitation but moving to a different measurement position, in this case $x = L_x/4, y = L_y/4$.

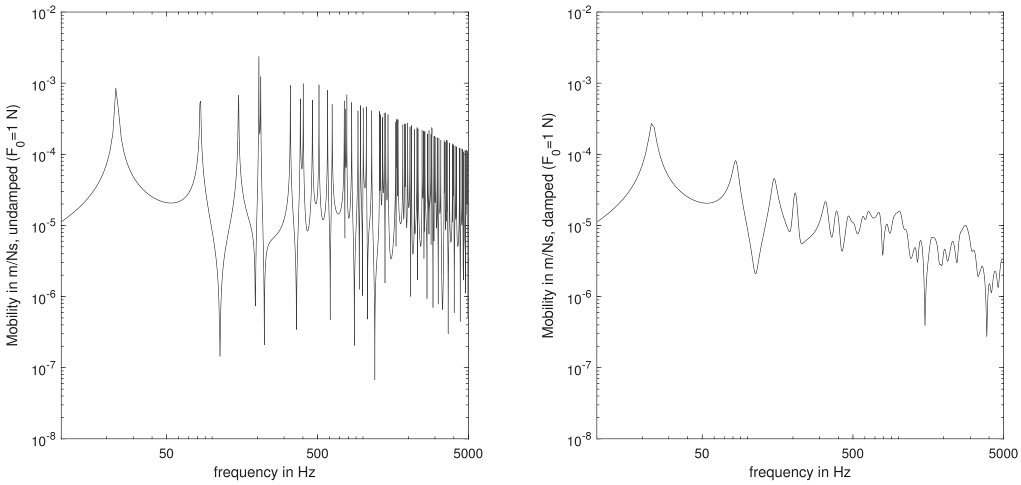

Figure 3.9: Transfer point mobility x=L$_x/4, y = L_y/2 (100-3plyCLTplate)$ $Left$:$\eta = 0.001$, Right:$\eta = 0.08$

3.3 Radiation efficiency

To understand the acoustic challenges facing CLT-constructions, the radiation efficiency can be calculated. Radiation efficiency "σ" is the ratio between radiated sound power of a structure and the power which theoretically would be radiated by a piston with the same surface area and velocity as the averaged velocity of the radiating structure of interest (Kropp, 2015).

$$\sigma = \frac{W}{\rho_0 c_0 S < v^2 >_{t,s}} \tag{3.16}$$

Calculating the average radiation efficiency of a plate is relatively straightforward with the simplified equations proposed by Leppington (Leppington, Broadbent, and Heron, 1982). The radiation of a plate is determined by the interaction of bending waves in the structure and the surrounding medium (i.e. air). Contrary to speed of sound in air, the phase velocity in a solid is going to vary with frequency. For a plate it is defined as

$$c_B = \sqrt[4]{\frac{B}{\rho S}\omega^2} \tag{3.17}$$

However, this is based on the assumption that the plate is thin. As the frequency increases, the wavelengths will become small enough to fit within the height of the plate. At that point it can no longer be assumed that the plate is thin. Thick plate theory is more complicated than thin plate and the modal behavior of a thick plate can not be easily modeled. The frequency at which this needs to be considered to make sure the error is not too large can be estimated as

$$f_{B(thin)} = \frac{0.05 c_L}{h} \tag{3.18}$$

where, c_L is the quasi-longitudinal wave speed and h the height of the plate. This frequency corresponds to where one sixth of the wavelength fits within the height of the plate. In order to consider the transition from thin to thick plate theory, a modified combined phase velocity can be calculated which considers the transverse wave influence on the resulting bending wave velocity when transitioning to a thick plate (Hopkins, 2007)

$$c_{B,thick} = \left(\frac{1}{c_B^3} + \frac{1}{\gamma^3 c_T^3} \right)^{-\frac{1}{3}} \tag{3.19}$$

where c_T is the transverse shear wave speed

$$c_{T,i} = \sqrt{\frac{E_i}{2\rho(1+\nu_i^2)}} \tag{3.20}$$

and $\gamma = 1.054$ for $\nu = 0.44$ and $\gamma = 1.358$ for $\nu = 0.64$. The γ's were interpolated from values given in Hopkins (2007). The phase velocity of thin and thick plates are shown in Figure 3.10. The thin plate theory renders a rather big error already around 1kHz in the minor direction.

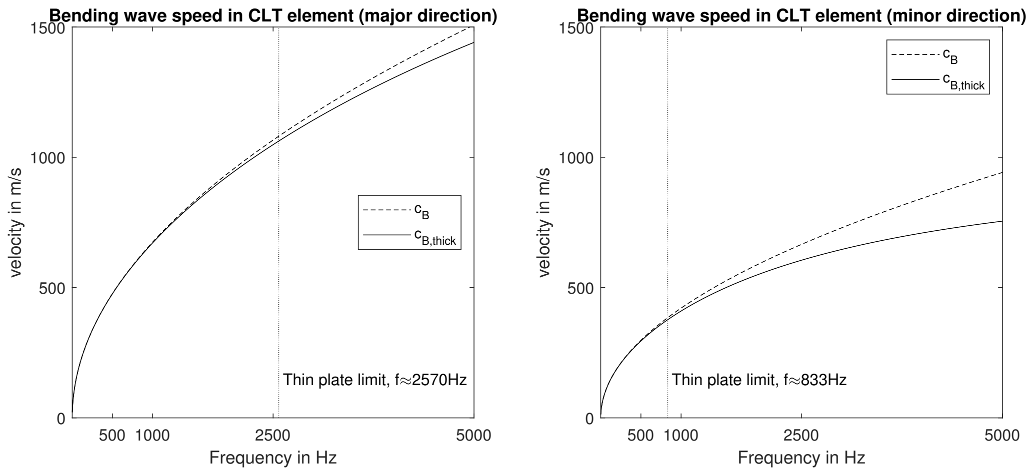

Figure 3.10: Phase velocity (100-3ply CLT plate)

The speed of bending waves in a plate will increase with frequency as seen in Figure 3.10. This means that there will only be one frequency for which the wavelength is the same in the solid and the surrounding fluid because the velocity of the wave is the same. This is called the critical frequency or coincidence, and around this frequency is where the plate will radiate best. Below coincidence, the wavelengths in the plate are shorter than those in the surrounding air, which means that no radiation occurs. Although, this is only true for the special case of an infinite plate. For a finite baffled plate some radiation will occur below coincidence as edge-radiation, caused by hydrodynamic short-circuiting. Above coincidence the wavelength in the plate will be longer than that of the corresponding frequency in air. This means that those waves will radiate at an angle in order to fit within the corresponding wavelength in air. The radiation efficiency above coincidence will go towards one (or 0 in dB) (Kropp, 2015).

CLT elements experience high damping. At low frequencies, the structural loss factor can reach 10 percent. When high damping is present some radiation might occur below the critical frequency that is not the result of edge radiation. In this case, it is because the waves decrease so much in amplitude with distance from excitation because of the high damping. Resulting in the half-cells not completely cancelling each other out in what is otherwise assumed as total intercell cancellation (Kou, Liu, and Tian, 2015). This needs to be taken into consideration when calculating radiation of CLT elements. Therefore a correction factor "C" is introduced for the calculated radiation efficiency below coincidence. The factor is based on the size of an equivalent square to the plate and the damping of the plate. The damping can increase radiation by 4 to 6 dB when going from 5 to 10 percent structural loss factor (Kou, Liu, and Tian, 2015). Figure 3.11 shows the regular case below coincidence where short-circuiting occurs everywhere on the plate except the edge, causing edge radiation. Figure 3.12 shows the same phenomena; but due to high damping there isn't total short-circuiting and therefore radiates some over the surface of the plate.

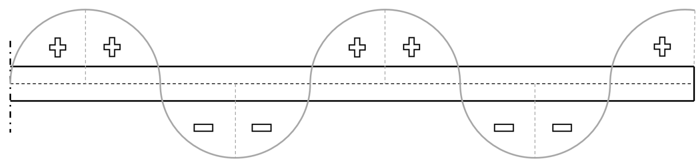

Figure 3.11: Edge radiation

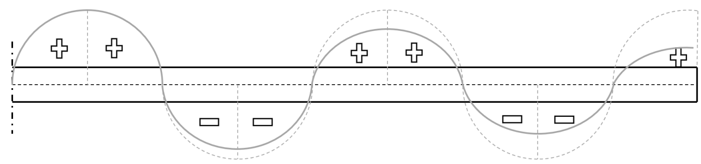

Figure 3.12: Radiation due to damping

The three radiation sections, below, around, and above coincidence are stated in Equation 3.21.

$$
\begin{aligned}
\sigma &= C\left(\frac{2}{\pi e k_B \mu\sqrt{\mu^2-1}}\right)\left[\ln\frac{\mu+1}{\mu-1}+\frac{2\mu}{\mu^2-1}\right] && \textit{when } f < f_c \\
\sigma &= \left(0.5-\frac{0.15L_y}{L_x}\right)\sqrt{k_B L_y} && \textit{when } f \approx f_c \\
\sigma &= \frac{1}{\sqrt{1-\mu^2}} && \textit{when } f > f_c
\end{aligned}
\tag{3.21}
$$

where

$$\begin{aligned} &L_x \geq L_y \\ &\mu = \sqrt{\frac{f_c}{f}} \\ &C = (22.81e - 5.13)\eta + (1.2 - 0.026e) \\ &e = 2L_xL_y/(L_x + L_y) \end{aligned} \tag{3.22}$$

To obtain the combined radiation efficiency of the plate

$$\sigma_{ortho}(\omega) = \frac{S}{\pi^2 n_d} \int_0^{\pi/2} \sigma(\omega,\theta) k_B \frac{\delta k_B}{\delta\omega} d\theta \tag{3.23}$$

where n_d is the modal density and the rate of change of the plate wave number with frequency is

$$k_B \frac{\delta k_B}{\delta\omega} = \frac{(k_{B,x}\cos\theta)^2 + (k_{B,y}\sin\theta)^2}{2\omega} \tag{3.24}$$

In Figure 3.13 the bending wave number is related to the wave number in air to show the critical frequency for different propagation directions in the timber element. It shows that the critical frequencies fall between 250-1000 Hz depending on angle (i.e. going from majot to minor direction). This frequency range is generally regarded as problematic for CLT elements as seen in Figure 3.1. The radiation efficiency has been calculated according to Equation 3.21 and is plotted in Figure 3.14.

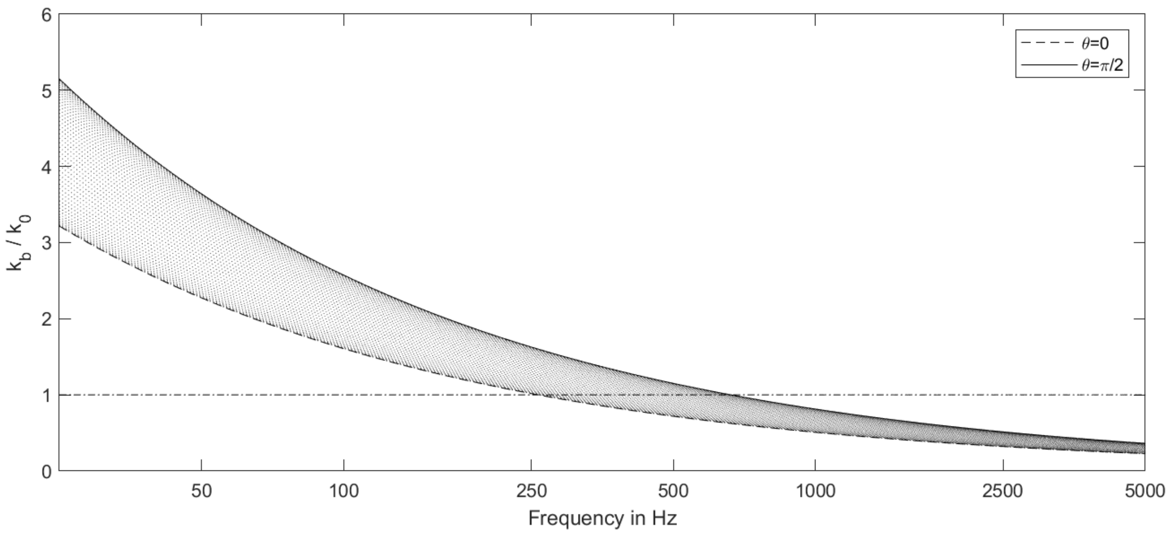

Figure 3.13: Coincidence of 100-3ply CLT plate

The radiation efficiency is then calculated for a finite number of angles between 0 and $\pi/2$ rad.

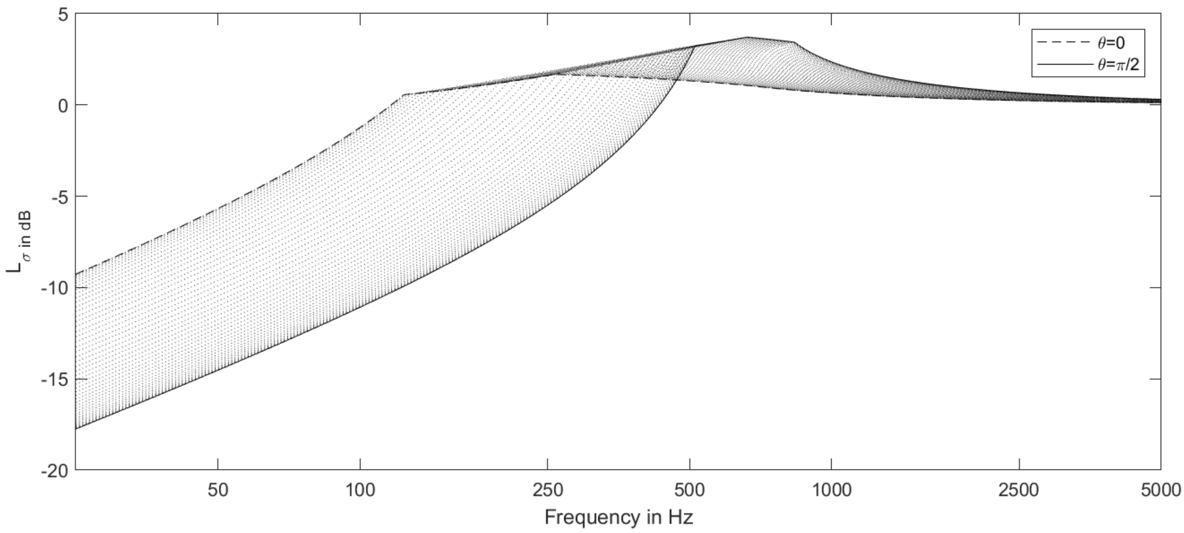

Figure 3.14: Radiation efficiency for a finite number of directions on the orthotropic 100-3ply plate

They are then combined according to Equation 3.23 for each frequency. This yields a wider peak than that of an isotropic model. This has been shown to be closer to what is seen when doing radiation measurements of CLT plates (Santoni, Schoenwald, Van Damme, Tröbs, and Fausti, 2016b).

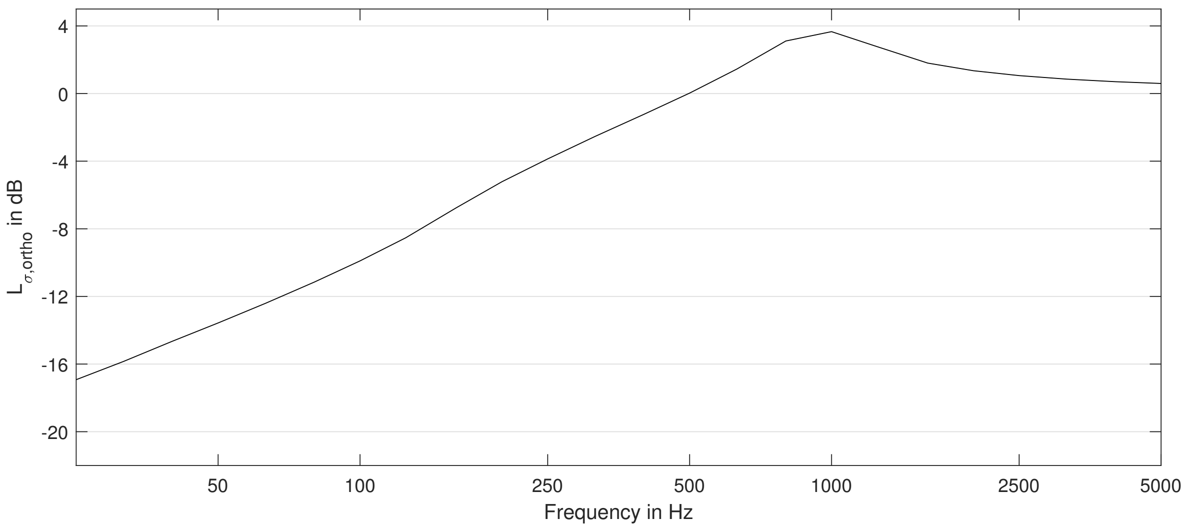

Figure 3.15: Combined radiation efficiency of 100-3ply cross laminated timber plate

In Figure 3.16 the 100mm-3ply element has been compared to the 100mm-5ply with material properties as stated in Table 3.1. The difference in bending stiffness of the two directions of the plate consisting of five layers is smaller and therefore more similar to an isotropic plate.

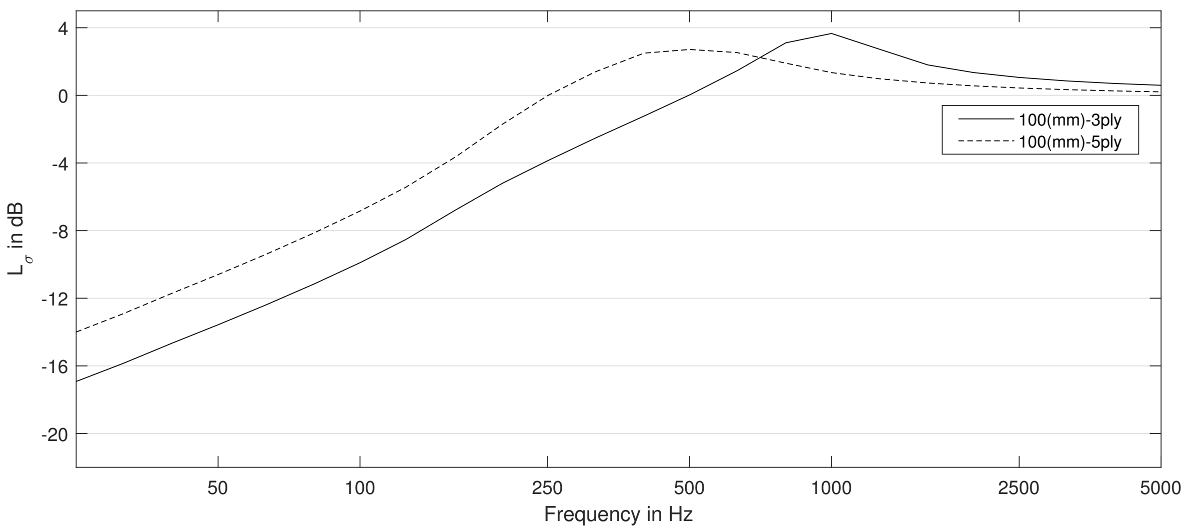

Figure 3.16: Radiation efficiency comparison 3-ply vs 5-ply

The effective method is compared to the previously presented method in Figure 3.17. The radiation efficiency is calculated according to Equation 3.21 but instead of calculating it for multiple angles of the plate, only one effective bending stiffness and one effective critical frequency are utilized as an isotropic model for an orthotropic material (Hopkins, 2007)

$$f_{c,eff} = \sqrt{f_{c,x} f_{c,y}} \tag{3.25}$$

The effective method does not showcase the same high radiation efficiency in low frequencies which is often the case with cross laminated timber.

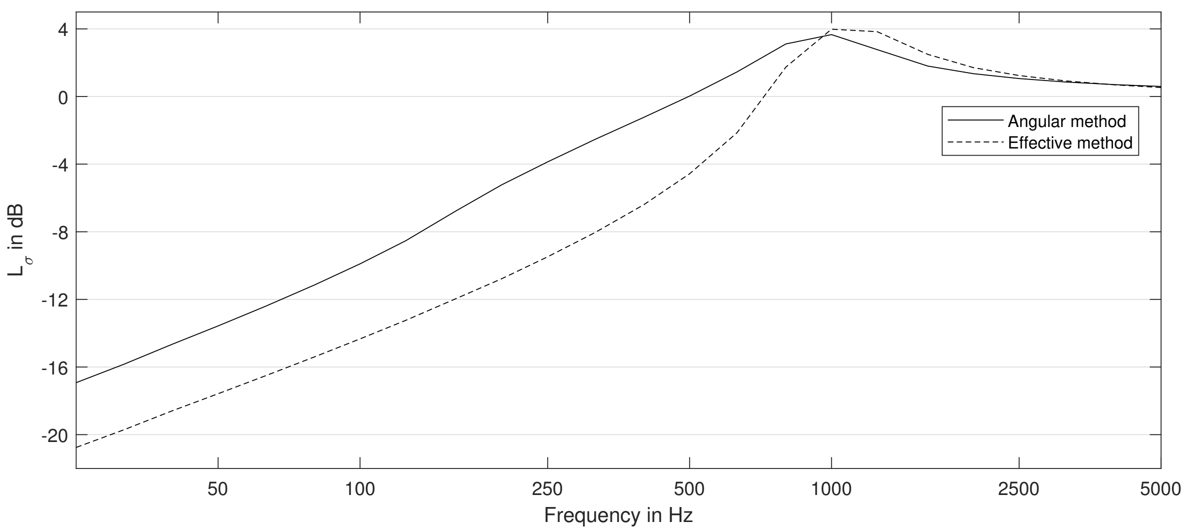

Figure 3.17: Radiation efficiency comparison proposed method vs effective

3.4 Vibration isolation

To isolate waves in a medium, a change in impedance is needed. The change in impedance can either be a change in geometry (orientation or cross section) which will be discussed in section 3.7 or a change in material (e.g. softer or harder). It is important to note that a change in impedance doesn't absorb the energy but reflects it. Some energy might be transformed into heat in the case of interlayers with high damping but the majority of the energy will either be transmitted through or reflected back into the system of the incoming wave. If the impedance of the interlayer is much lower than that of the connected elements and if the thickness of the interlayer is much smaller than the wavelength in the interlayer, then the transmission factor for longitudinal waves is defined as

$$\tau_L = \frac{1}{1 + \frac{1}{4}\left|\frac{ESL}{\lambda_L/(2\pi)E_e S_e}\right|^2} \tag{3.26}$$

where, E, S and L are the material and geometric properties of the two connected beams and E_e and S_e for the elastic interlayer. The closer the Young's modulus of the interlayer is to the connected elements, the more vibrations will be transmitted. This is why these types of interlayers are soft i.e. have a low Young's modulus.

For bending waves the transmission factor can be estimated according to

$$\tau = 1 - \left|\frac{-v + \epsilon^2 v^3 + \epsilon^2 v^4/2}{(v + \epsilon^2 v^3) - j(4 + v - \epsilon^2 v^3 - \epsilon^2 v^4/2)}\right|^2 \tag{3.27}$$

where $\epsilon^2 v^2 << 1$ and

$$\epsilon = \frac{E_e h}{E2L} \quad and \quad v = \frac{EL2\pi}{E_e \lambda_B} \tag{3.28}$$

If $v >> 4$ then the reduction index of the elastic interlayer for bending waves can be directly estimated as

$$R_B = 10\log\left[1 + \left(\frac{1 - \epsilon^2 \nu^3}{2}\right)^2\right] \tag{3.29}$$

The reduction indexes are plotted in Figure 3.18. It shows that there is a frequency for the bending wave reduction where total transmission takes place. The analysis has been done for a common interlayer used in CLT-constructions (E_e=1.8 MPa). The total transmission occurs around 50 Hz, and below that frequency the interlayer isn't really providing much isolation. The isolation starts becoming somewhat effective above 100 Hz. Figure 3.18 shows that longitudinal waves are somewhat easier to control.

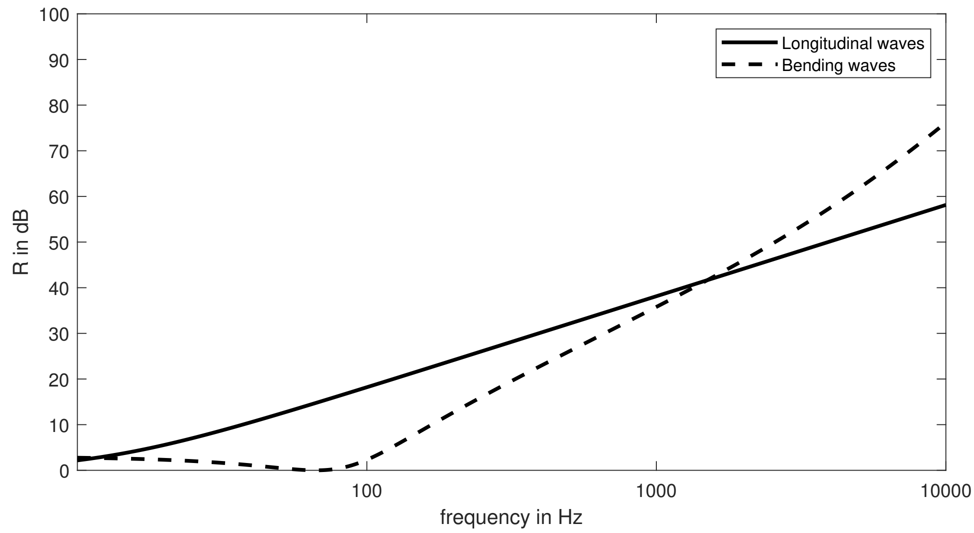

Figure 3.18: Reduction index of elastic interlayer

Figure 3.19 is an instruction of how to install an elastic interlayer between two CLT elements with the aim to reduce flanking transmission. It is sometimes preferred to have exposed CLT elements, mainly because of architectural reasons discussed in section 1.4. It is favorable under those circumstances to pull back the elastic interlayer a bit and place a sealant along the side of the interlayer that would be exposed to potential fire in order to increase resistance.

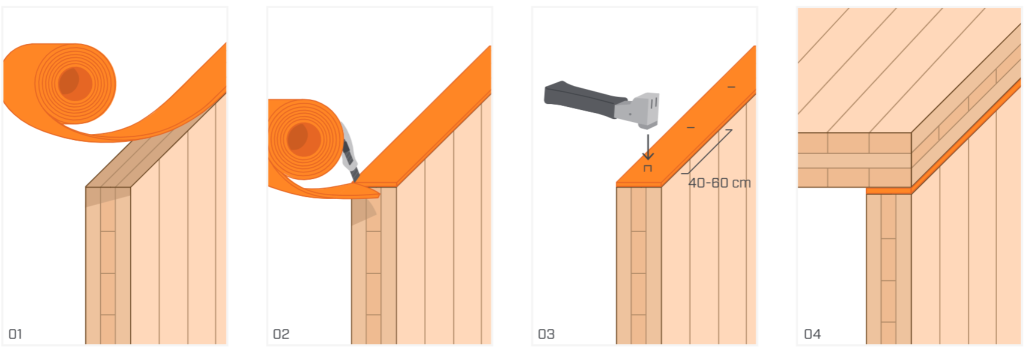

Figure 3.19: Elastic interlayer installation
Credit: Rothoblaas soundproofing solution (Rothoblaas, 2018)

There are several ways to measure the effectiveness of an isolator. Transmissibility is the level difference (e.g. displacement, velocity) between both sides of an isolator. Insertion loss is a similar ratio of the difference in transmission with and without the isolator (Kropp, 2015). Three CLT T-junctions with different fastening systems are presented in the figures below. The junctions have been measured with and without the elastic interlayers as part of the Flanksound project by Rothoblaas (Rothoblaas, 2018). The measured K_{ij} is based on the velocity level difference between elements, as well as some correction factors which will be discussed in detail in section 4. However, when only looking at the difference between the same junction, it works well enough for this comparison because the rest of the factors cancels out. Only the straight path from one wall to another will be presented here. The reason is that the walls are more difficult to treat acoustically since adding layers infringes on usable room area.

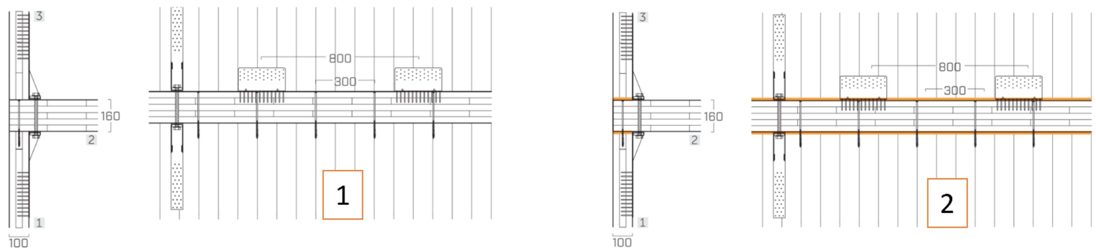

f (Hz)	100	125	160	200	250	315	400	500	630	800	1000	1250	1600	2000	2500	3150
$K_{13,1}(dB)$	23.8	26.9	16.6	21.5	21.5	17.8	15.1	18.4	24.6	25.5	25.3	24.8	27.5	34.9	35.1	42.1
$K_{13,2}(dB)$	24.4	21.8	16.0	22.5	18.9	20.2	16.9	23.2	27.6	29.5	29.9	28.7	31.9	42.1	44.3	48.2
Ins. loss (dB)	0.6	-5.1	-0.6	1.0	-2.6	2.4	1.8	4.8	3.0	4.0	4.6	3.9	4.4	7.2	9.2	6.1

Figure 3.20: Insertion loss of elastic interlayer in T-junction (1)
Credit: Rothoblaas soundproofing solutions (Rothoblaas, 2018)

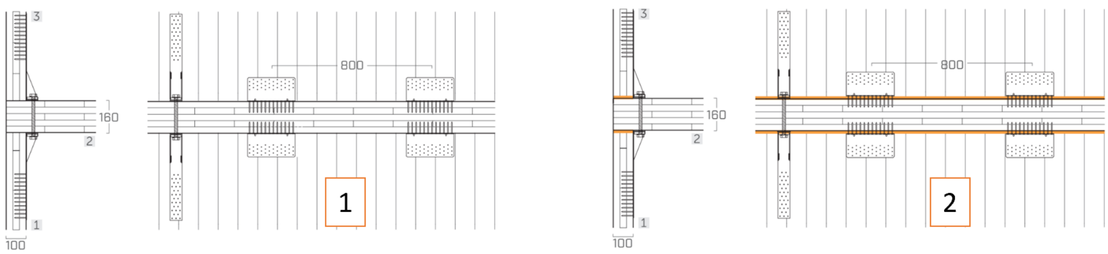

f (Hz)	100	125	160	200	250	315	400	500	630	800	1000	1250	1600	2000	2500	3150
$K_{13,1}(dB)$	26.9	26.7	18.3	20.6	19.1	12.9	8.8	12.4	15.1	17.5	19.7	22.8	24.6	30.7	34.3	32.0
$K_{13,2}(dB)$	23.6	27.1	16.5	18.7	18.0	14.2	10.6	14.6	16.7	22.0	24.0	26.6	29.4	31.4	34.0	32.5
Ins. loss (dB)	-3.3	0.4	-1.8	-1.9	-1.1	1.3	1.8	2.2	1.6	4.5	4.3	3.8	4.8	0.7	-0.3	0.5

Figure 3.21: Insertion loss of elastic interlayer in T-junction (2)
Credit: Rothoblaas soundproofing solutions (Rothoblaas, 2018)

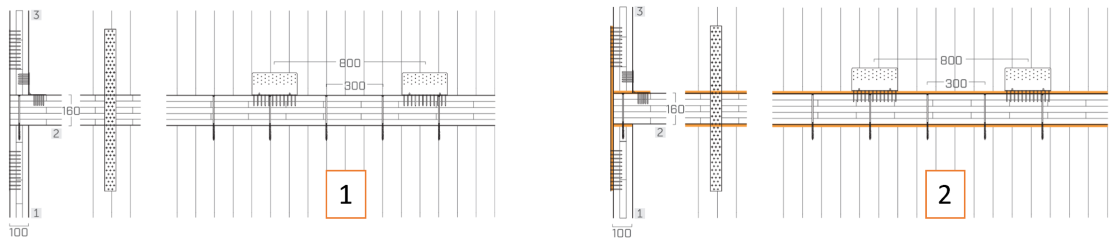

f (Hz)	100	125	160	200	250	315	400	500	630	800	1000	1250	1600	2000	2500	3150
$K_{13,1}(dB)$	22.5	25.3	15.7	16.5	15.0	12.6	13.4	15.8	21.1	18.6	19.3	18.8	23.5	29.0	27.5	32.3
$K_{13,2}(dB)$	23.9	24.5	18.3	20.6	16.3	18.2	19.4	19.6	25.7	27.2	25.6	21.9	24.5	41.7	44.9	49.0
Ins. loss (dB)	1.4	-0.8	2.6	4.1	1.3	5.6	6.0	3.8	4.6	8.6	6.3	3.1	1.0	12.7	17.4	16.7

Figure 3.22: Insertion loss of elastic interlayer in T-junction (3)
Credit: Rothoblaas soundproofing solutions (Rothoblaas, 2018)

There is no data provided below 100 Hz (where total transmission in regards to the elastic interlayer probably occurs). The elastic interlayer does not seem to be particularly effective in the frequency range of concern ~100-800 Hz. This can in part be explained by the elastic interlayer in the junction being shortcut by rigid paths i.e. screws. The study "Flankenübertragung bei Massivholzkonstruktionen" provided possible optimized fastening systems. The study suggests that one such fastener can be an angle-connector with elastic interlayer between the metal and building elements (example: Figure 3.23). It showed significant improvement compared to the same fastener without elastic interlayer (Dolezal, Bednar, and Teibinger, 2008).

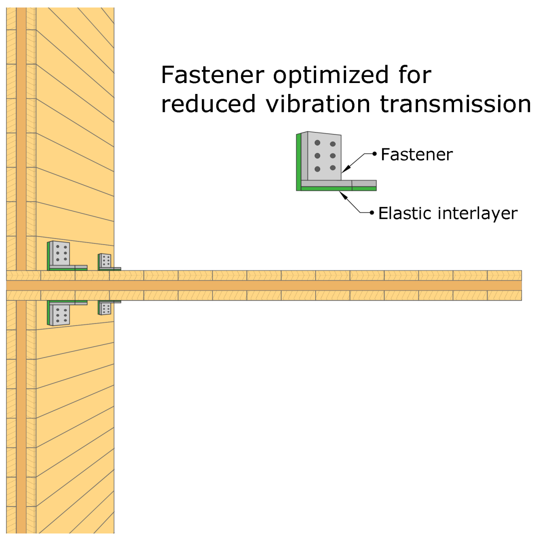

Figure 3.23: Optimized fastener with elastic interlayer

The type of screw and the density of connection points are understood to have a big impact on flanking transmission (Rothoblaas, 2018). In mid to high frequencies, the more dense the metal connections are, the more vibrations transmit from one element to the other. It is not noticeable in low frequency since the connections are rather small compared to the wavelength. Figure 3.24 showcase the difference in a L-junction with connections of 200 mm step size versus 400 mm (Rothoblaas, 2018).

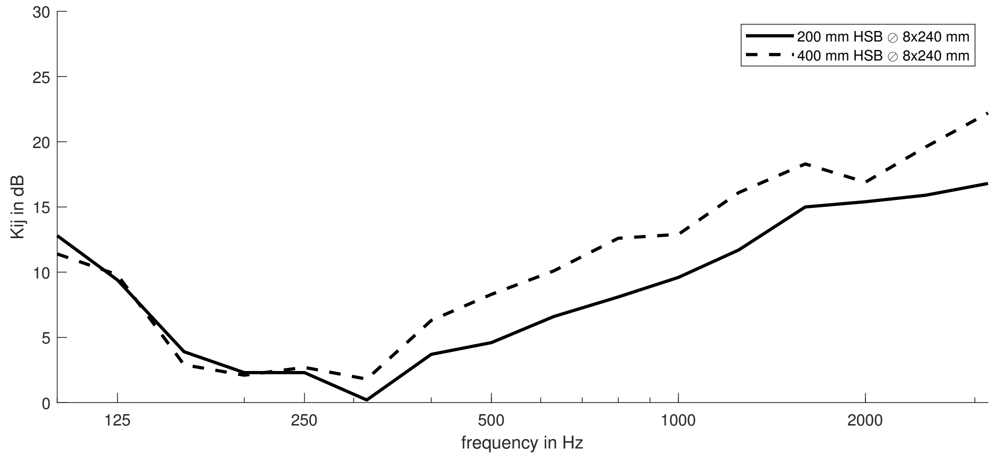

Figure 3.24: Transmission through screws (Lab measurement)

More importantly, there are several dips in insertion loss; in some frequency bands it even goes to negative values that can not be explained by vibrations bypassing through connections. In those frequencies it's actually worse to have the elastic interlayer. This is likely because the wall and interlayer act like a mass-spring system. The system then has an eigenfrequency, which likely exists in the frequency range studied e.g. at 125 Hz for Figure 3.20. This enables the wall to vibrate even more than if it was rigidly connected to the junction.

Another challenge with elastic interlayers is that the whole idea is that it is soft, but when constructing higher buildings the load is going to increase with every level. There will be a limit to how soft of a material can be utilized when the load increases. Therefore a stiffer material will have to be used. This will move the total transmission in Figure 3.18 up in frequency, making it less effective. Two ways to combat this are either to make the interlayer thicker or narrower. Neither of these solutions are great for a structure under high load since it makes it less stable. With increasingly higher CLT-constructions there is going to be a point at which elastic interlayers simply aren't effective at the lower levels of the building. Some alternatives to elastic interlayers have been suggested. Bending wave transmission can be dealt with if perpendicular forces can be reduced within the junction. One idea is to move away from rigid connections and replace them with a connection seen in Figure 3.25. This would give in to momentum and horizontal forces acting on the junction but still transfer the static vertical force and thereby minimize the bending wave transmission to the connected element (Ljunggren, 2011). The connection has been proven to be relatively effective, but questions remain concerning the stability of such a construction and if the connection needs to be stiffened by e.g. metal rods to handle wind loads it might mitigate the original gains.

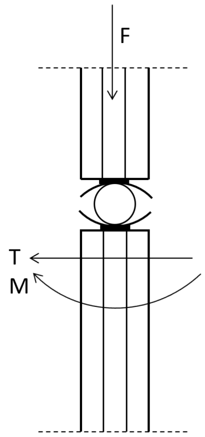

Figure 3.25: Rolling connection

Something that is rarely discussed in reference to CLT is the usage of blocking mass. The idea is to create an impedance change, causing reflection like an elastic interlayer but this time using a high density material instead of low density. The transmission coefficient of a blocking mass can be calculated according to

$$\tau_{BM} = 1 - \left| \frac{\mu + \theta^2\mu^3 + \theta^2\mu^4/2}{(\mu + \theta^2\mu^3) - j(4 + \mu - \theta^2\mu^3 - \theta^2\mu^4/2)} \right|^2 \tag{3.30}$$

where

$$\mu = \frac{m}{\rho S \lambda / 2\pi} \tag{3.31}$$

and

$$\theta = \frac{m}{\rho S}\sqrt{\frac{\Theta}{m}} \tag{3.32}$$

where Θ is the polar moment of inertia of the blocking mass. The blocking mass has a frequency where there is total transmission just like the elastic interlayer. This time however the frequency where total reflection occurs is visible for the blocking mass. In the case of Figure 3.26 the elastic interlayer is compared to a slab of steel with the same thickness. The blocking mass is only more effective around the point of total reflection. Therefore it is not a viable alternative even if one could justify the extra cost and weight.

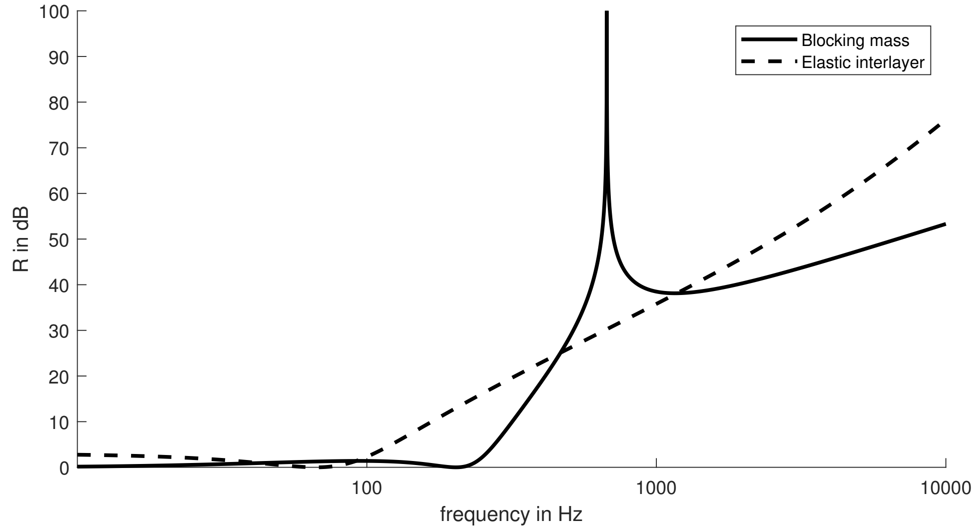

Figure 3.26: Reduction index blocking mass and elastic interlayer (h=0.025 m)

3.5 Damping

Reflection caused by impedance change is a way to isolate vibrations but doesn't actually decrease the vibration energy. If that energy needs to go away, it has to be transformed into some other energy e.g. heat. This is achieved by damping in the structure. Material damping is complicated. It is not a material constant like others. Material damping is a function of the history of the material such as the previous deformations and aging. Therefore, studying the damping of a structure can tell a lot about changes in the material over time (Kropp, 2015).

Santoni, Schoenwald, Van Damme, Tröbs, and Fausti (2016b) measured the loss factor of a 80mm-3ply CLT element. The result was damping that decreased with frequency. The measured loss factor can be viewed in third octave bands in Table 3.2

f (Hz)	50	63	80	100	125	160	200	250	315	400	500	630	800	1000	1250	1600	2000	2500	3150
η	0.08					0.07			0.06	0.05	0.04	0.03							

Table 3.2: Measured loss factor of CLT element

3.6 Load

The question of how external loads affect junction transmission becomes important when timber starts being utilized in taller buildings. In Figure 3.27, three L-junctions with and without resilient interlayers, and with and without external load applied are presented (Timpte, 2016). In the frequency range of interest ∼100-800 Hz the external load has a much greater impact on the vibration transmission than the elastic interlayer.

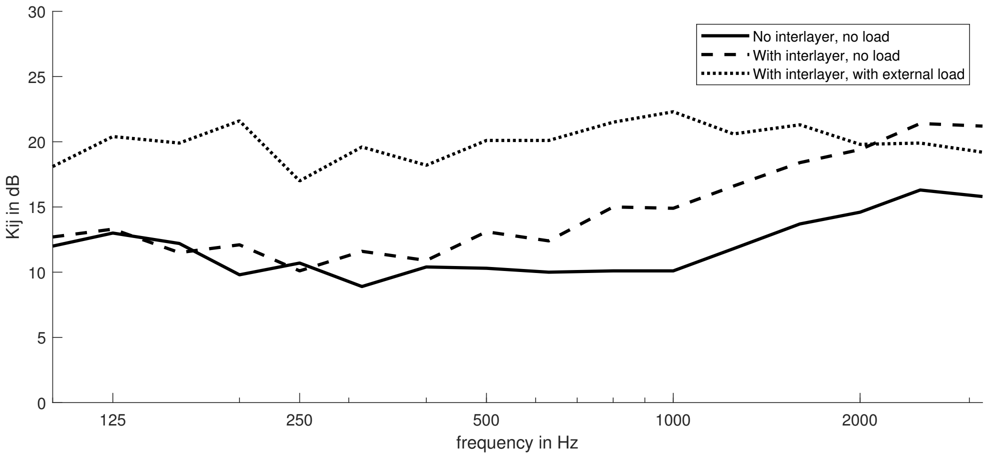

Figure 3.27: Vibration transmission through junction exposed to external load (Lab measurement)

Bard, Davidsson, and Wernberg (2010) measured the sound transmission between apartments in a multi-storey CLT-construction. The experiment involved a tapping machine placed on the floor of the sending room. Accelerometers were placed on the floor in the sending room to measure the input, as well as the floor in the adjacent room, the ceiling or the wall in the room below to measure the response, depending on the measured vibration path. This was done for level 2 and 5 (sending room). All measurements showed a higher vibration reduction in the higher levels except for ultra low frequencies (<10 Hz). The difference between the floor levels were greatest in the horizontal vibration path. The vibration reduction of the floor to floor flanking path went from an attenuation of -23 dB on level 5 to -12 dB on level 2, in the 1kHz third-octave band; an 11 dB difference. In lower frequencies (around 40 Hz) the difference between levels of the building was about 3-4 dB, with level 5 performing better. The flanking path floor to wall below showed a 2-3 dB difference in almost all frequency bands above 10 Hz, again with the lower level attenuating less vibrations.

3.7 Junction transmission

This section explores what happens with waves propagating through a junction. It deals with longitudinal and bending waves. An L-junction is examined. As the different wave types travel from one element to the other, some waves will transmit through and some will be reflected because of the change in geometry. Some will transform from one wave type to other types of waves.

The bending wave reduction caused by a difference in thickness of two beams connected as an L-junction can be estimated as (Kropp, 2015)

$$R = 20\log\left(\sigma^{-5/4} + \sigma^{5/4}\right) - 3dB \tag{3.33}$$

where σ represents the change in geometry, $\sigma = \frac{h_2}{h_1}$. If the two connected elements are of the same material and same thickness, then R=3dB. If the elements are the same material but one is 150 mm and the other is 100 mm, which is a common configuration for CLT walls connected to a CLT floor, then R=4dB. If $\frac{h_2}{h_1} = 2$, then R=6 dB.

For the idealized case of two beams connected in an L-junction of the same material and same thickness (which is the case of the measurement in Section 6.1) then the transformation of an incident bending wave can be estimated according to Equation 3.34 and 3.35. τ_{XY} denotes transformation of wave type X to wave type Y in the connected beam. ρ_{XY} denotes transformation of wave type X to wave type Y as it is reflected back into the beam of the incident wave. B is for bending wave type and L is for longitudinal wave type. Transformation from bending waves can be estimated for the idealized case as

$$\begin{aligned}
\tau_{BB} &= \frac{1+2\beta^2}{2+6\beta+9\beta^2} \\
\rho_{BB} &= \frac{1-2\beta^2}{2+6\beta+9\beta^2} \\
\tau_{BL} &= \frac{5\beta+8\beta^2}{2+6\beta+9\beta^2} \\
\rho_{BL} &= \frac{\beta}{2+6\beta+9\beta^2}
\end{aligned} \tag{3.34}$$

and for longitudinal waves

$$\begin{aligned}
\tau_{LB} = \tau_{BL} &= \frac{5\beta+8\beta^2}{2+6\beta+9\beta^2} \\
\rho_{LB} = \rho_{BL} &= \frac{\beta}{2+6\beta+9\beta^2} \\
\tau_{LL} &= \frac{\beta^2}{2+6\beta+9\beta^2} \\
\rho_{LL} &= \frac{2}{2+6\beta+9\beta^2}
\end{aligned} \tag{3.35}$$

where $\beta = 2h/\lambda_B$.

The resulting bending wave coefficients are plotted over frequency in Figure 3.28. In low frequencies, bending waves are either almost completely reflected back or transmitted through as bending waves. In high frequencies, most bending waves are transmitted through as longitudinal waves in the connected beam. Only a small portion of the energy is ever reflected back as longitudinal waves.

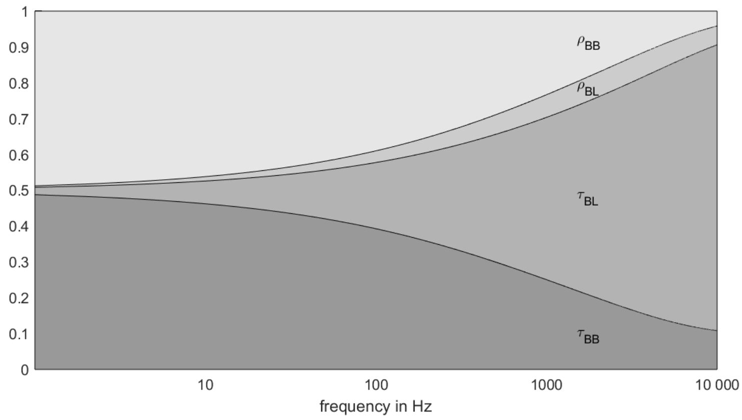

Figure 3.28: Bending wave transmission and reflection in rigid L-junction

Figure 3.35 showcase the same coefficients but for incident longitudinal waves. In low frequencies, longitudinal waves are mostly reflected back as longitudinal waves. In higher frequencies, most are transmitted through as bending waves. Very little energy is reflected back as bending waves or transmitted through as longitudinal waves.

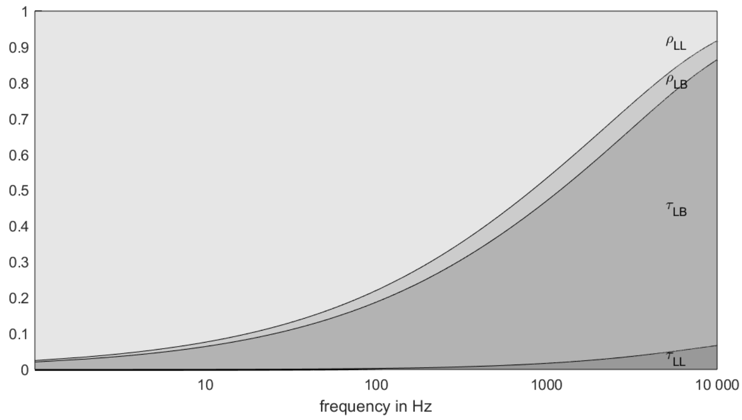

Figure 3.29: Longitudinal wave transmission and reflection in rigid L-junction

What is more relevant though are T and X-junctions, since these are the most common junctions when dealing with sound transmission from one room to another in a multi-story building. A similar, albeit more cumbersome evaluation than the one made for the L-junction, can be made for a cross-junction by following the procedure detailed in Chapter 6.2.3 of Cremer and Heckl's "structure-borne sound" (Cremer, Heckl, and Ungar, 1988). The case studied is an incoming bending wave from member 1 in the cross-junction. The material is of the same material (100-5ply and 150-5ply as detailed in Table 3.1). Most of the energy is reflected back as bending waves in member 1. Only in high frequencies does transformation to longitudinal waves occur and it almost only occurs in the horizontal members. When the members are of the same thickness, the transmission of bending waves is relatively even between the three connected beams in the frequency range of interest. When the vertical members have a different thickness compared to the horizontal members, the transmission to the second vertical beam drastically decreases. That energy is instead reflected back into member 1. The bending wave transmission to the horizontal beams decreases slightly compared to the case with the same height.

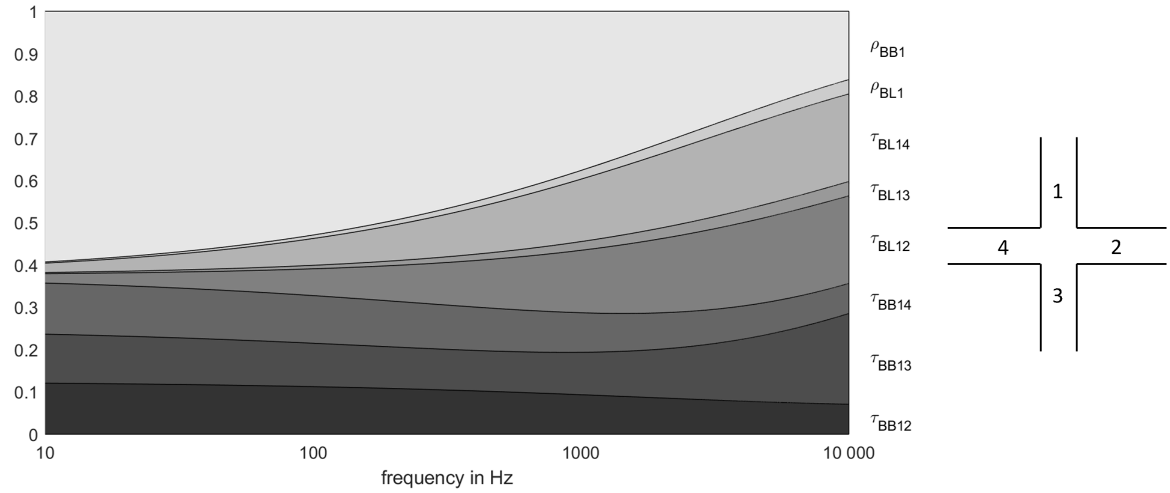

Figure 3.30: Bending wave transmission and reflection in X-junction
Horizontal members: 150-5ply, Vertical members: 150-5ply

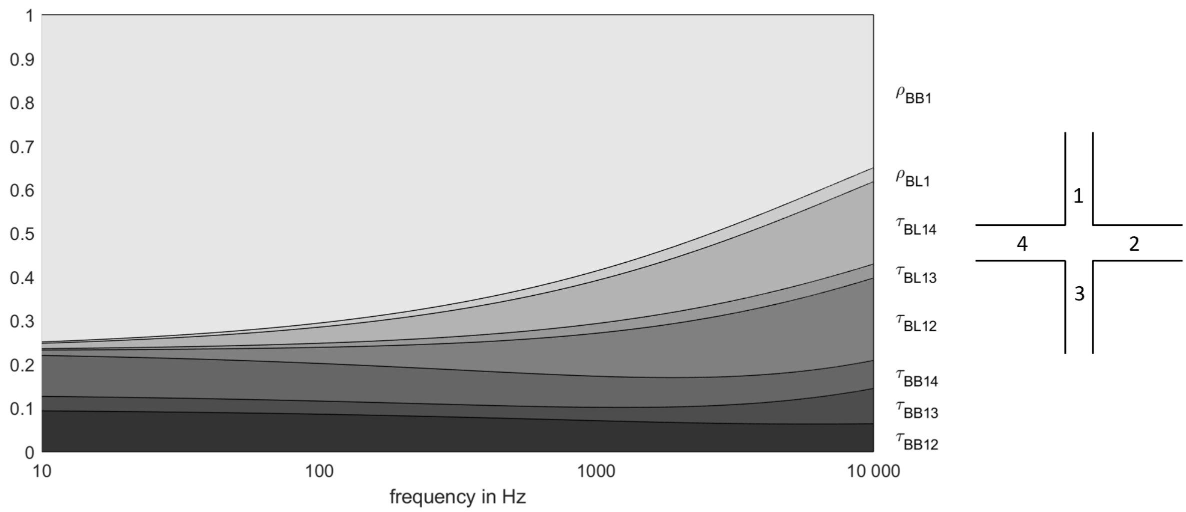

Figure 3.31: Bending wave transmission and reflection in X-junction
Horizontal members: 150-5ply, Vertical members: 100-5ply

4
Vibration reduction index

The field measurements is carried out in accordance with the standard ISO 10848-1 (ISO, 2000) as this thesis work is limited to measuring the K$_{ij}$ of chosen connections. Appendix E of ISO 12354-1 (ISO, 2017) mentions that although ISO 10848-1 is for controlled lab measurements, it is feasible to apply the same method for in-field measurements.

The prediction method described in ISO 12354-1 was originally developed for concrete and masonry elements and was therefore considered a good enough approximation for CLT when it gained popularity.

K$_{ij}$ is the factor that relates to the type of joint that is present and determines the flanking contribution when calculating the total noise transmission between two rooms as described in ISO 12354-1 (ISO, 2017). It is a quantity that is less predictable and more difficult to determine than for example the reduction index of a wall (Crispin, Mertens, Blasco, Ingelaere, Van Damme, and Wuyts, 2004).

The quantity K$_{ij}$ is related to the vibrational power transmission over a junction. It is defined as:

$$K_{ij} = \bar{D}_{v,ij} + 10log\frac{l_{ij}}{\sqrt{a_i a_j}} \quad [dB] \tag{4.1}$$

where $\bar{D}_{v,ij}$ is the direction averaged velocity level difference on the surface of element i and j, in decibels. It is obtained from the arithmetic mean of the differences between the velocity level on the surface of element i and j, $D_{v,ij}$ (when element i is excited) and $D_{v,ji}$ (when element j is excited), in decibels

$$\bar{D}_{v,ij} = \frac{D_{v,ij} + D_{v,ij}}{2} \tag{4.2}$$

l_{ij} is the common length of the junction between element i and j, in meters. a_i and a_j is the equivalent absorption length of element i and j respectively, in meters. It is used to describe all of the absorption at the plate boundaries in one single equivalent totally absorbent length. The equivalent absorption length is given by:

$$a = \frac{2.2\pi^2 S}{c_0 T_s}\sqrt{\frac{f}{f_{ref}}} \tag{4.3}$$

where T_s is the structural reverberation time of the element i or j, in seconds. S is the area of element i or j, in square meters. f is the center band frequency, in

Hertz. f_{ref} is the reference frequency; f_{ref}=1000 Hz. c_0 is the speed of sound in air, in meters per second. (ISO, 2017)

4.1 Standard K_{ij} estimation

Annex E in ISO 12354-1 provides K_{ij}-estimates for a number of junctions. The estimations are based on empirical values. When the standard was developed it was geared towards concrete and masonry structures. The deciding factor of the estimations is the possible mass difference of the connected elements. An estimation of a rigid T-junction is defined as (ISO, 2017)

$$\begin{aligned} K_{13} &= 5.7 + 14.1M + 5.7M^2 \; dB \; (Straight\ path) \\ K_{12} &= 5.7 + 5.7M^2 \; dB \; (Perpendicular\ path) \end{aligned} \tag{4.4}$$

where $M = 10log(m'_i/m'_j)$. For a T or X-junction with flexible interlayers

$$\begin{aligned} K_{13} &= 5.7 + 14.1M + 5.7M^2 + 2\Delta_1 \; dB \; (Straight\ path) \\ K_{12} &= 5.7 + 5.7M^2 + \Delta_1 \; dB \; (Perpendicular\ path) \end{aligned} \tag{4.5}$$

where $\Delta_1 = f/f_1$ for $f > f_1$ where $f_1 = 125Hz$.

If the connected elements are the same material and height, then M=0. In Figure 4.1 that case is plotted for junction with elastic interlayer.

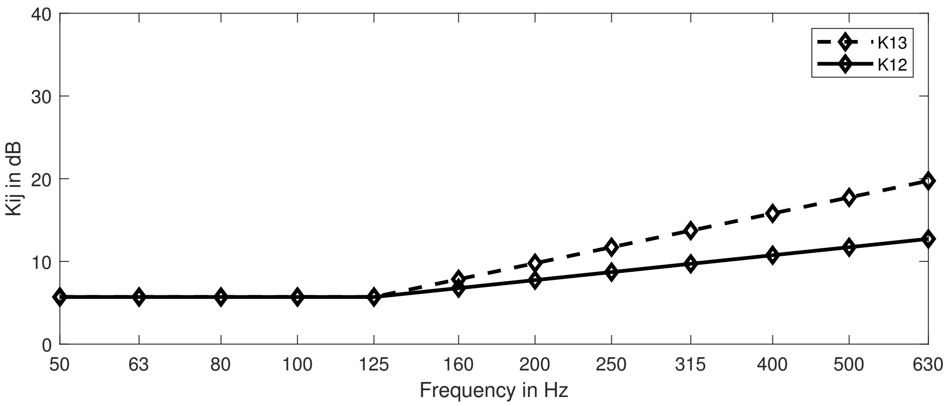

Figure 4.1: ISO 12354-1 annex E estimation for junction with flexible interlayers

The estimations of Annex E in ISO 12354-1 can be compared to the analytic solution presented in section 3.7. The comparison is presented in Figures 4.2 and 4.3. The standard estimations are modeled as a rigid x-junction as described in Annex E of ISO 12354-1

$$\begin{aligned} K_{13} &= 8.7 + 17.1M + 5.7M^2 \; dB \; (Straight\ path) \\ K_{12} = K_{14} &= 8.7 + 5.7M^2 \; dB \; (Perpendicular\ paths) \end{aligned} \tag{4.6}$$

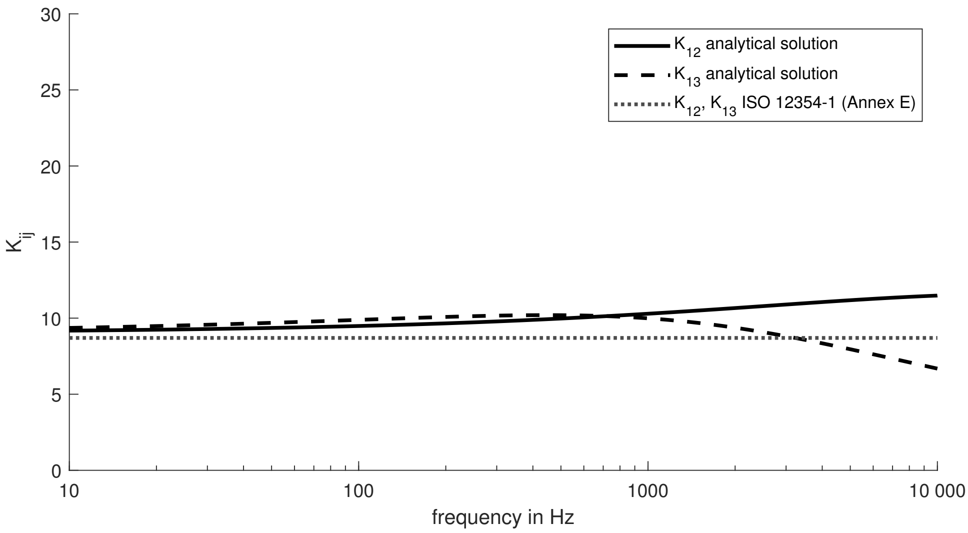

Figure 4.2: ISO 12354-1 annex E estimation for CLT junction with members of the same thickness (vertical members=150 mm, horizontal members=150 mm) compared to analytic solution in section 3.7

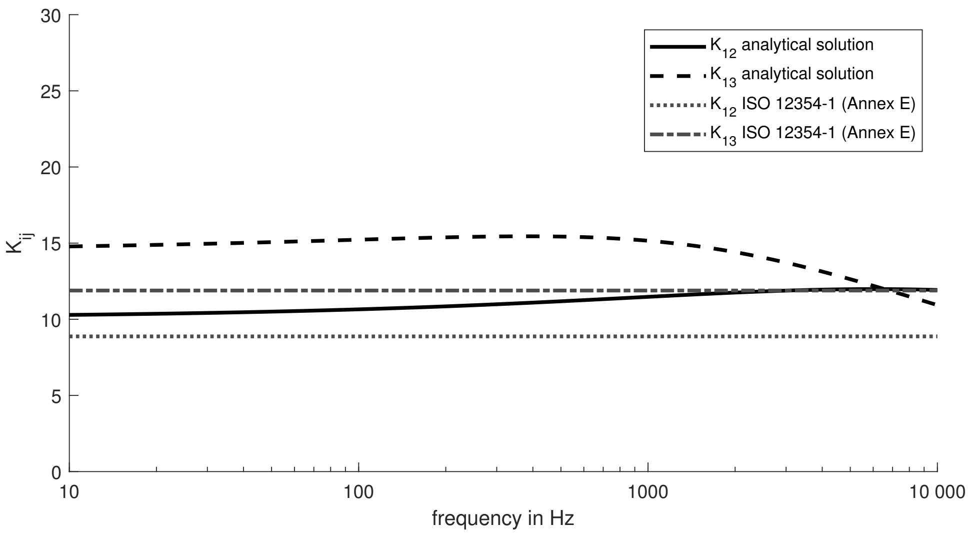

Figure 4.3: ISO 12354-1 annex E estimation for CLT junction with members of different thicknesses (vertical members=100 mm, horizontal members=150 mm) compared to analytic solution in section 3.7

5

Finite element model

A quick finite element analysis to test the potential of using computer software to estimate the vibration behavior of CLT is performed. It is done for the simplest possible junction, a wall-wall L-junction with 3 ply CLT elements. The dimensions of the analyzed junction can be seen in Figure 5.1. The finite element model (FEM) is limited by the fact that it builds on the idea of stepping through the model divided into a mesh grid. A higher frequency analysis requires a finer grid since the wavelengths become smaller. The FE-analysis is therefore capped at 800 Hz to reduce calculation time.

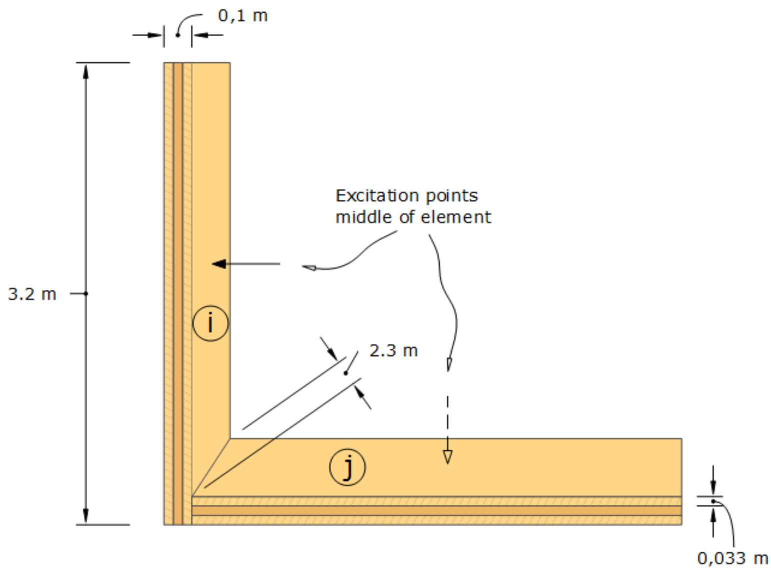

Figure 5.1: Dimensions of finite element model

Figure 5.2 showcase the first six mode shapes of the studied L-junction.

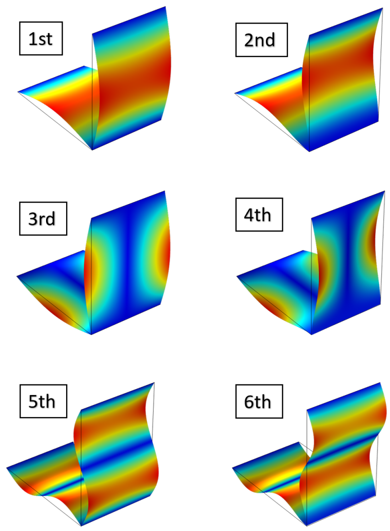

Figure 5.2: First six mode shapes of L-junction

The software used is COMSOL multiphysics 5.4. Each wall is made up of three solid orthotropic plates. The material properties of the middle layer of each wall is rotated 90° to simulate the composition of a CLT element. The material data used is that of an "Eastern Cottonwood" as detailed in Table 5.1. The parameters used, are elastic moduli, shear moduli and Poisson's ratio as well as density ρ=480 kg/m^3. The indexes corresponds to how they relate to the fibers of the tree where L is longitudinal, T is tangential, and R is radial. Damping is set to η=0.2 (Vardaxis, 2014).

E_L	10,340 MPa
E_R	858 MPa
E_T	486 MPa
G_{LR}	786 MPa
G_{LT}	538 MPa
G_{RT}	155 MPa
ν_{LR}	0.34
ν_{LT}	0.42
ν_{RT}	0.29
η	0.2
ρ	480 kg/m^3

Table 5.1: Material data used in FEM (Handbook, 2010)

Adhesion between lamellas and fastening method between elements is not taken into consideration. Excitation is simulated as a point load in the middle of each element respectively.

Figure 5.3 and 5.4 illustrate the geometry of the model and the mesh used.

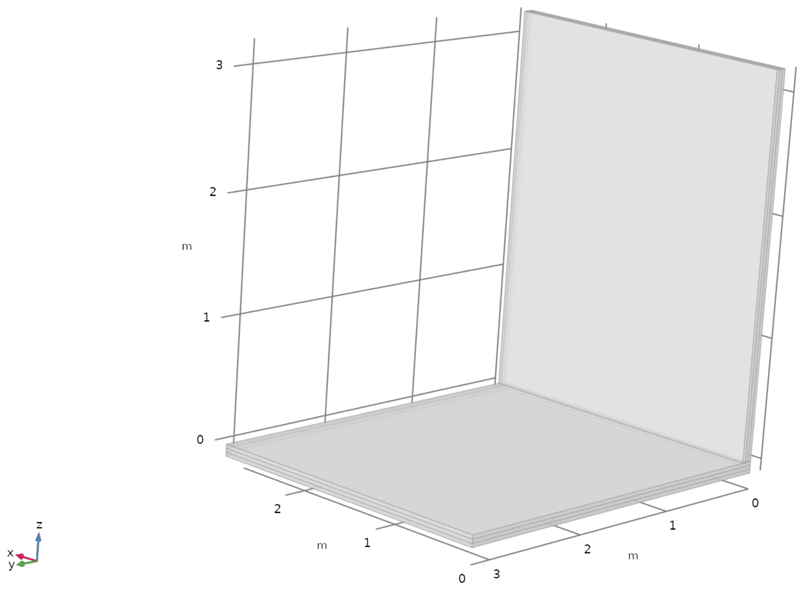

Figure 5.3: FEM geometry

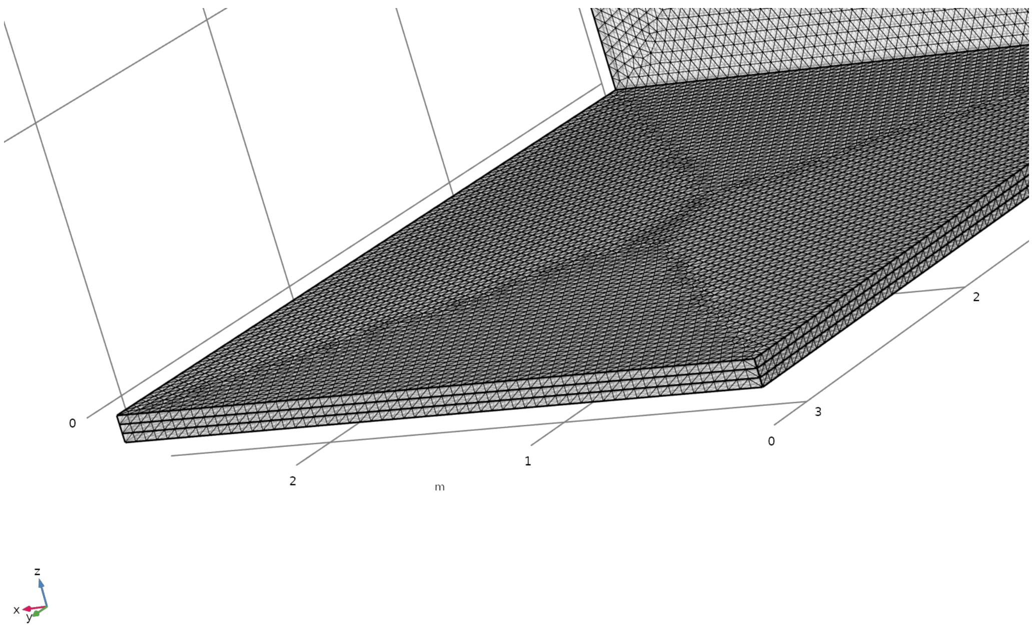

Figure 5.4: FEM mesh

The maximum and minimum mesh grid element size is 0.065 m and 0.013 m resp. which is enough to ensure at least six points per wavelength. The time required for one calculation is 19 h 45 min. Since two calculations are needed, one for each element excited, the total calculation time ends up being approximately 40 hours.

The forced vibration analysis of the FEM outputs the average surface velocity amplitude of each element. This is then calculated according to Section 4 and plotted alongside two similar measured L-junctions in Figure 5.5. The structural reverberation time T_S is related to the loss factor as (Kropp, 2015)

$$T_S = \frac{2.2}{\eta f} \tag{5.1}$$

The finite element model fits rather well with the measured junctions.

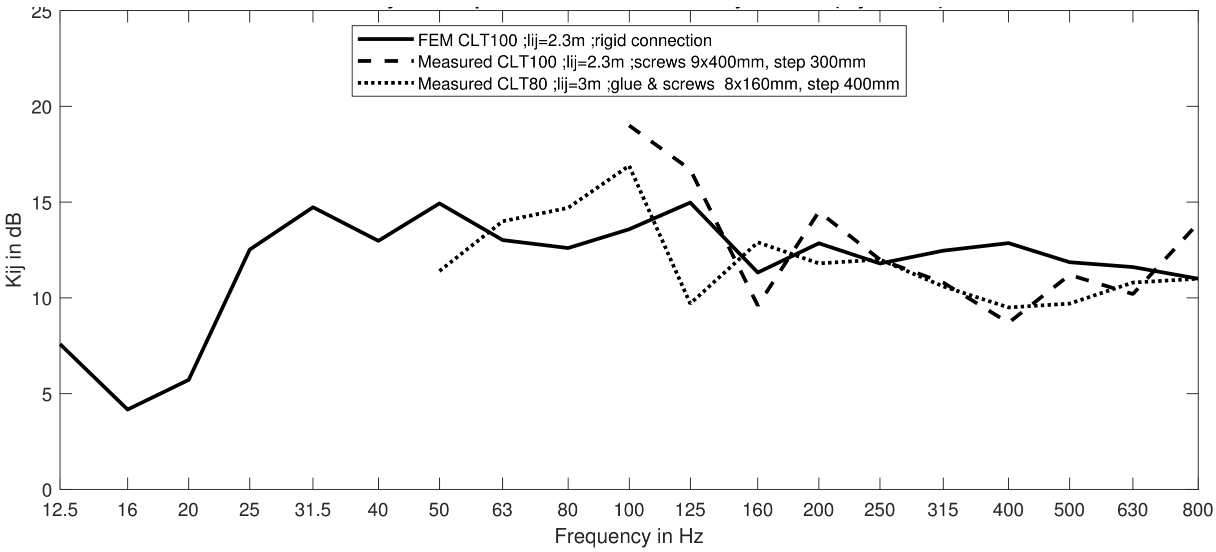

Figure 5.5: K_{ij}-comparison FE-model vs. similar lab measured L-junctions

6

Field measurement

The following section describes the steps needed to measure the vibration reduction index of a junction in-field. The standard ISO 10848 details the amount of accelerometer and excitation positions that are needed as well as placement range.

The input excitation needs to be 10 dB higher than the measured velocity level of the background noise on the receiving element for every frequency band. ISO 10848-1 details two ways of measuring the $D_{v,ij}$. The stationary direct and the transient direct method. The first excites the elements by the use of an electrodynamic shaker with steady-state signal or a tapping machine whereas the latter utilizes an impact/force hammer. When comparing the two, and the average difference between the methods was about 1 dB with 8 junction-paths with rigid connection measured; which is not significant (Crispin, Mertens, Blasco, Ingelaere, Van Damme, and Wuyts, 2004).

If transient method is used then the hammer should be swung with an equal amount of force every time over a surface of 1-2 m^2 at a frequency of 1-2 Hz over 20-30 s. If background noise is prominent, a higher frequency of impact is required. The response of both the element being excited and the connected element should be recorded at the same time since it is difficult to ensure a stable input when swinging a hammer.

Stationary excitation can be achieved with a shaker. An MLS (Maximum-Length-Sequence) or sine sweep can be used to excite the structure. These inputs are good for maximizing the signal-to-noise ratio. For each measurement an integration time should be chosen so that no significant velocity level change occurs.

Since CLT is what is referred to as a type A element in the standard, only three excitation point are required. Because CLT can be considered homogeneous, either side of the element can be used for measurements. The positioning of the accelerometers and excitation should be random but still within a constricted area based on the relation to adjacent elements and accelerometers/ excitation (ISO, 2000):

- 0,5 m between excitation points and the test element boundaries
- 1,0 m between different excitation points
- 1,0 m between excitation points and the junction under test
- 1,0 m between excitation points and the associated measurement positions
- 0,25 m between measurement positions and the test element boundaries
- 0,5 m between the individual measurement positions for each associated excitation position

This thesis utilizes the transient method. The measurement-chain is very simple. It consists of four accelerometers connected to a digital acquisition system with four channels. The elements are excited by the impact of a mass e.g hammer, sledge hammer or dropping mass. The input is then recorded according to annex B of ISO 10848 (ISO, 2000) by placing one of the accelerometers 30 mm from the point of impact. The three remaining accelerometers measure the response. The measurement chain can be seen in Figure 6.2. Descriptions of some of the symbols used in the following figures can be seen in Figure 6.1

Figure 6.1: Symbols

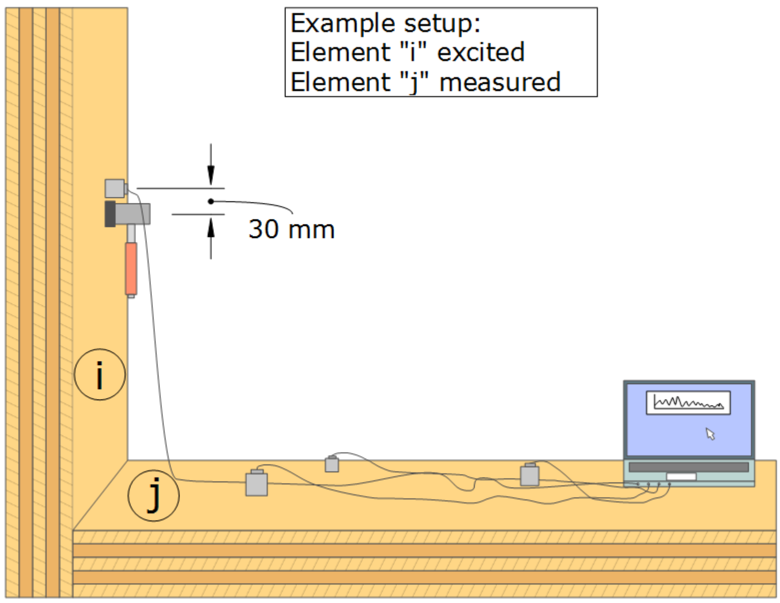

Figure 6.2: Measurement chain

The amount of measurements for one junction quickly adds up. Table 6.1 specifies how many measurements are needed, assuming one accelerometer measures input and three measures response. The last line of the table is the product of the above lines. Not included in the table is that every data-point of every excitation also is an average of X amounts of impulses.

Type of junction	**L**	**T**	**X**
Number of elements to excite	2	3	4
Excitations per element	3	3	3
Accelerometers per excitation	4	4	4
Elements to measure per excitation	2	3	4
Number of data points	48	108	192

Table 6.1: Measurement data points

One measurement that slightly complicates the practicality of the setup when working in-field instead of lab environment is when an element should be excited in a separate room from the element in which the response is measured. In practice, this is very difficult to achieve in a realized building for the transient method. This requires a deviation from the standard. Instead of measuring the response of the element being excited and the response of the element connected at the same time, the input will be recorded and used to normalize the responses of any given recording. However, in measurement 1 (section 6.1), yet another deviation is done. Low signal-to-noise ratio caused by long cables and impracticality of measuring at a construction site made any recording of input and output simultaneously impossible. The lack of input measurement is compensated by a greater number of impulses, in the pursuit to create a good enough average input.

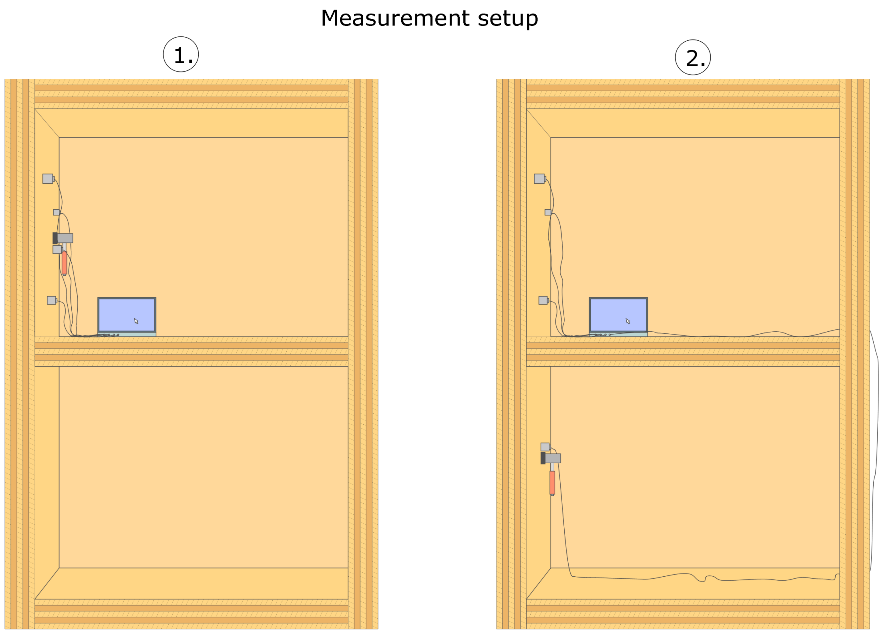

Figure 6.3: Measurement setup

The accelerometers need to be fastened to the element it's measuring. ISO 10848-1 states that the accelerometer is to be mounted directly onto the element and that the fixing should be stiff in the normal direction of the test element. It mentions beeswax as a convenient option but that it might result in issues in high frequencies. Since the thesis is mainly concerned with low to mid frequencies and there is no possibility to drill/screw in the elements in-field this is seen as a valid trade off.

The setup will include a force sledge hammer to excite the elements, as opposed to a shaker or dropping mass. The material of the tip of the hammer plays a big role in what kind of input can be achieved. This is demonstrated in Bruel and Kjaers product sheet for their biggest impact hammer type used for exciting larger structures such as buildings (Figure 6.4). It details the input force over frequency for different material tips.

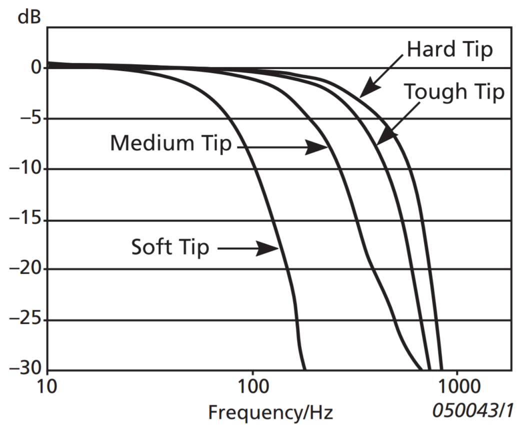

Figure 6.4: Input force over frequency for different impact hammer tips
Source: BruelKjaer, Product data: Heavy-duty Impact Hammers Types 8207, 8208 and 8210

It is important that measurements are taken in the reverberant field of the plate in order to measure the actual response of the structure and not the input. The distance from excitation is detailed in the standard but to be sure, it can be calculated for the material in question. The distance from the excitation point where the energy of the direct field equals the energy in the reverberant field is

$$r_{rd} = \frac{\omega \eta S}{4\pi c_B} \tag{6.1}$$

As seen in Figure 6.5, the 1 m between excitation and measurement position is suitable for the material and frequency range in question.

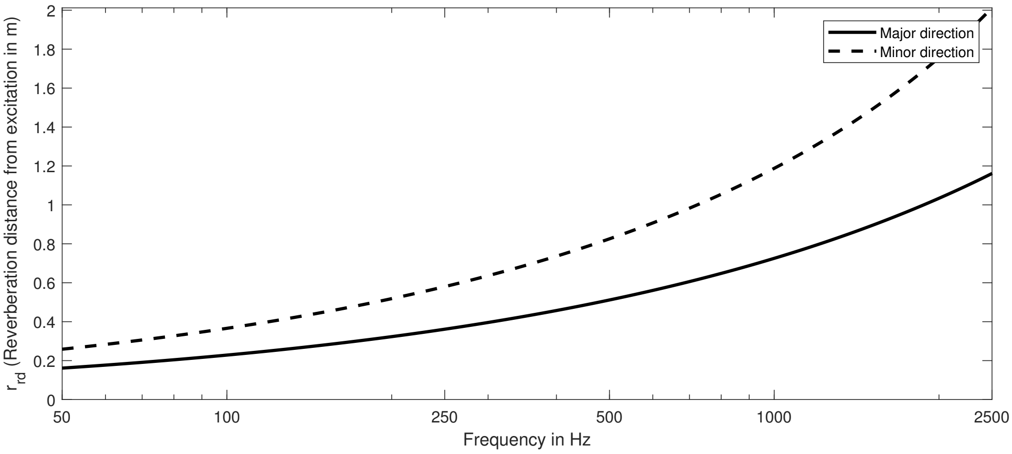

Figure 6.5: Distance to reverberant field from excitation on plate

The vibration field is not perfectly diffused over the surface of the plate. There will be more variation in lower frequencies. A standard deviation of the spatial variation of the velocity level on a plate can be estimated according to

$$\sigma_{dB} \approx \sqrt{43log\left(1+\left[\left(1+\frac{3}{\pi M}\right)\left(1+\frac{N_s}{\pi M}\right)\right]\right)} \tag{6.2}$$

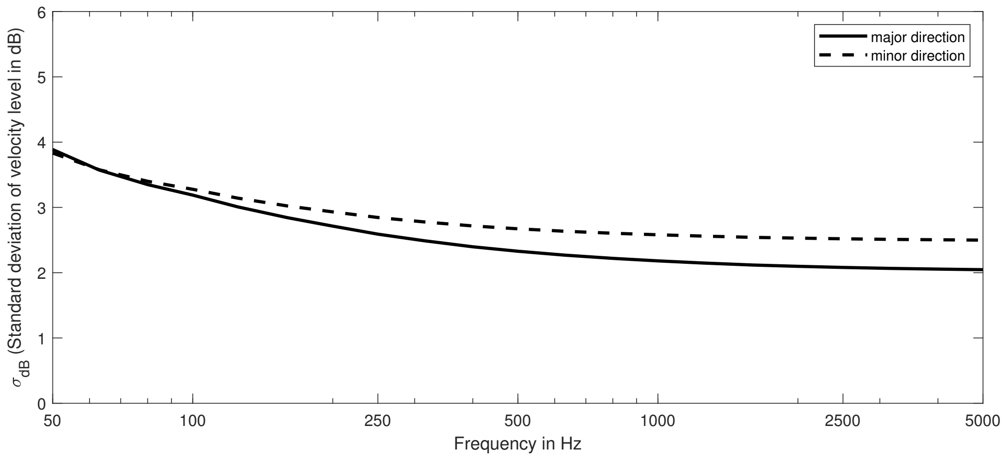

Figure 6.6: Spatial variation standard deviation of velocity level on plate

The bending waves will decrease in amplitude with distance, d, from excitation due to damping. These losses can be described for different frequencies with a level decrease for bending waves as (Kropp, 2015)

$$\Delta L_{=} \frac{4.3\pi\eta d}{\lambda_B} \tag{6.3}$$

and for longitudinal waves as

$$\Delta L_{=} \frac{8.7\pi\eta d}{\lambda_L} \tag{6.4}$$

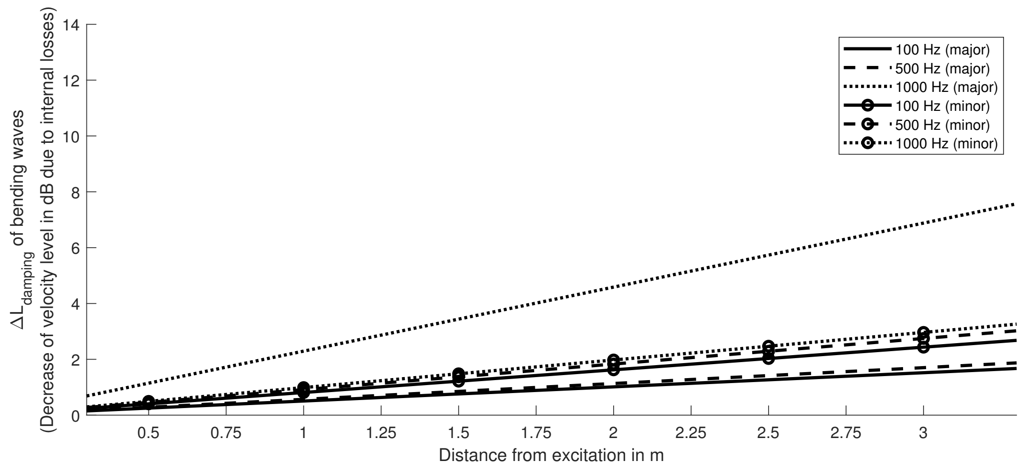

Figure 6.7: Decrease in vibration level with distance from excitation due to damping

6.1 Measurement 1

The first measurement took place in a building still under construction. This enabled easier excitation of the elements since there weren't any finished surfaces to be worried about when fixing accelerometers and swinging the hammer. All CLT elements were 5-ply with a total thickness of 130 mm (30-20-30-20-30). The internal walls were double leaf with mineral wool in between and an outer layer of gypsum on each side (Figure 6.9).

In total three junctions were measured. One T-junction and two X-junctions. The T-junction was an external wall-floor junction. The two X-junctions were internal wall-floor junctions. The two internal junctions were identical with the exception of room sizes and position in the building. The external junction and one of the internal junctions were located between level five and six, while the third junction was between level four and five. The junctions and their dimensions can be seen in Figure 6.8.

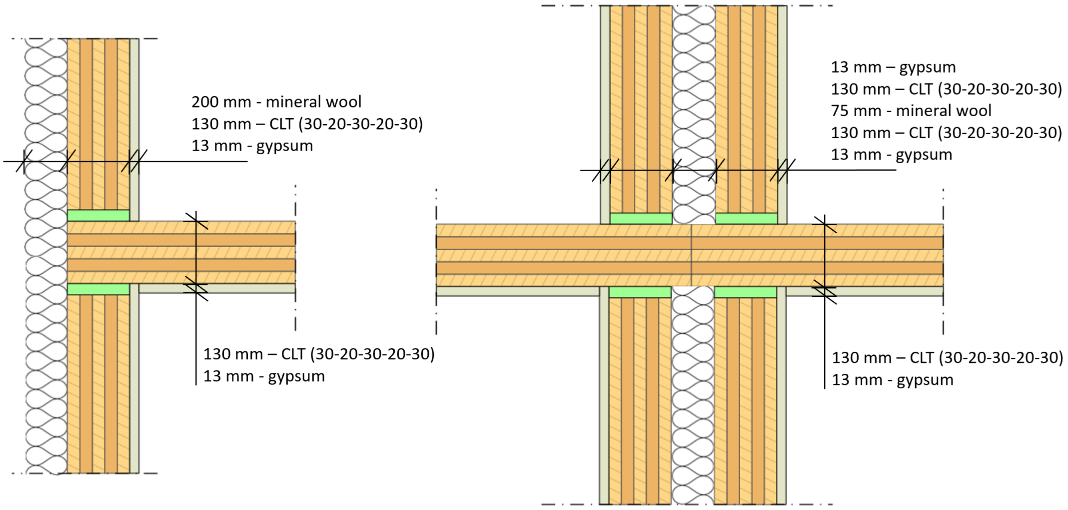

Figure 6.8: Measured junction dimensions

Figure 6.9: Measurement 1: Internal wall

The external wall was one CLT element with inner layer of gypsum and outer layer of mineral wool (Figure 6.9).

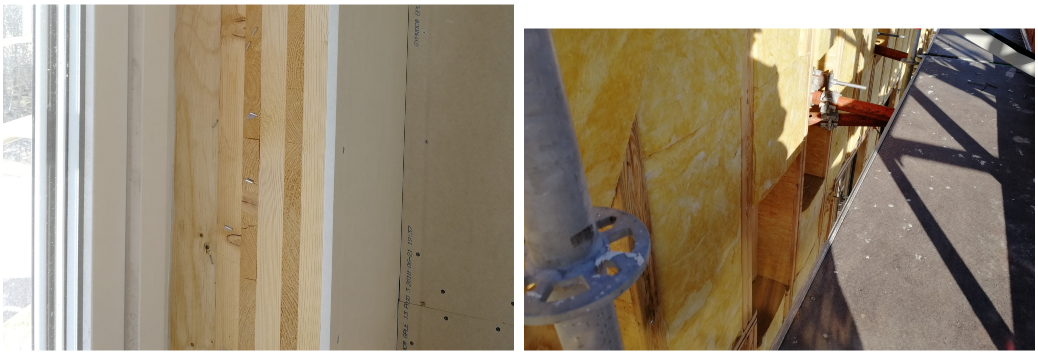

Figure 6.10: Measurement 1: External wall

The floor was exposed timber and the ceiling had one layer of gypsum (Figure 6.11).

Figure 6.11: Measurement 1: Floor

The connections of the elements were angle brackets with elastic interlayers between the metal and timber. This is similar to the proposed optimized fasteners discussed in Section 3.4.

Figure 6.12: Measurement 1: Connections

A strip of elastic interlayer is placed at the connection between the wall and the floor. The elastic interlayer in question has a dynamic E-modulus=1.86 MPa.

Figure 6.13: Measurement 1: Elastic interlayer

The setup consisted of three accelerometers, one amplifier, one DAQ, one computer, and one sledge hammer. The full list can be found in Table 6.2. A picture of the setup can be seen in Figure 6.14.

Instrument	Model
3 Accelerometers	B&K 4338
Amplifier	B&K 2692
DAQ Hardware	NI 9234
Hammer	Dytran 5803

Table 6.2: Measurement 1: Equipment list

Figure 6.14: Measurement 1: Setup

Because of the nature of the measurement specimen there were some limiting factors which restricted the ability to follow the standardized measurement method. The main problem was the amount of cable noise produced when measuring the impact hammer with a very long cable. This made the input measurement useless. The result was that the input was not measured and instead replaced with more hits to increase the probability of a stable average input to the system. This also ensured the measurement could be performed within the time-frame and made for a method which was easier to execute in a construction site. The elements were excited 40 times during a 40 second measurement i.e. with a 1 Hz excitation frequency. This was done for six accelerometer positions per elements. The data points for one junction are:

Number of elements to excite	3
Excitations per element	2
Accelerometers per excitation	3
Elements to measure per excitation	3
Number of data points	54

Table 6.3: Measurement data points

If each impulse recorded is taken into account the data points can be multiplied by 40 and the total amount of impulses for one junction is 2160.

Figure 6.15 presents the auto spectrum of the signals that were recorded for accelerometers placed on element i for one of the junctions. Three signals for each element excited as well as a fourth background measurement. This provides the upper frequency limit, where the signals are less than 10 dB higher than background noise. This has resulted in capping the frequency analysis at 630 Hz in third-octave bands. Figure 6.15 is calculated from the signals provided in Figure 6.16. The signals have been modified so that the outliers of the upper and lower 10th percentile are removed and filled in by an average impulse.

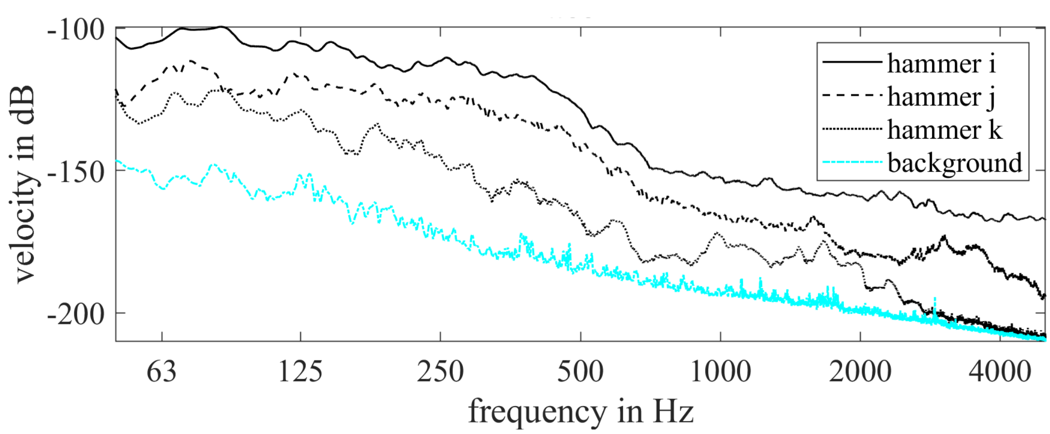

Figure 6.15: Measurement 1: velocity level over frequency of accelerometer example (accelerometer i)

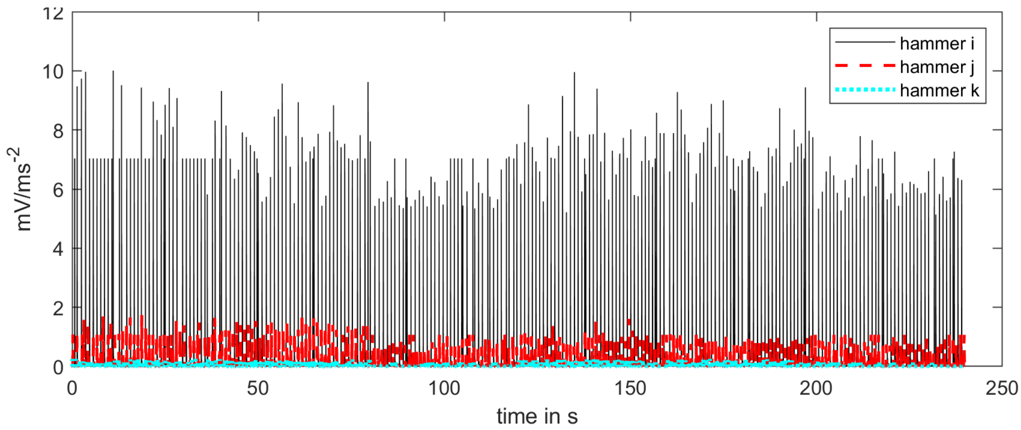

Figure 6.16: Measurement 1: velocity amplitude over time of accelerometer example (accelerometer i)

Figures 6.17 and 6.18 represent the energy put into the system by the hammer as measured by an accelerometer 30 mm from the hammer hit. This has been performed on a wall as well as a floor element.

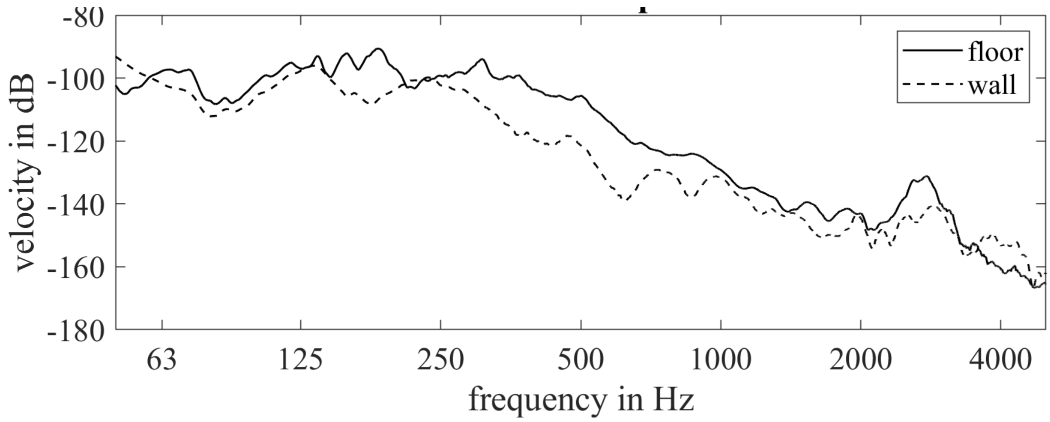

Figure 6.17: Measurement 1: velocity level over frequency of hammer example

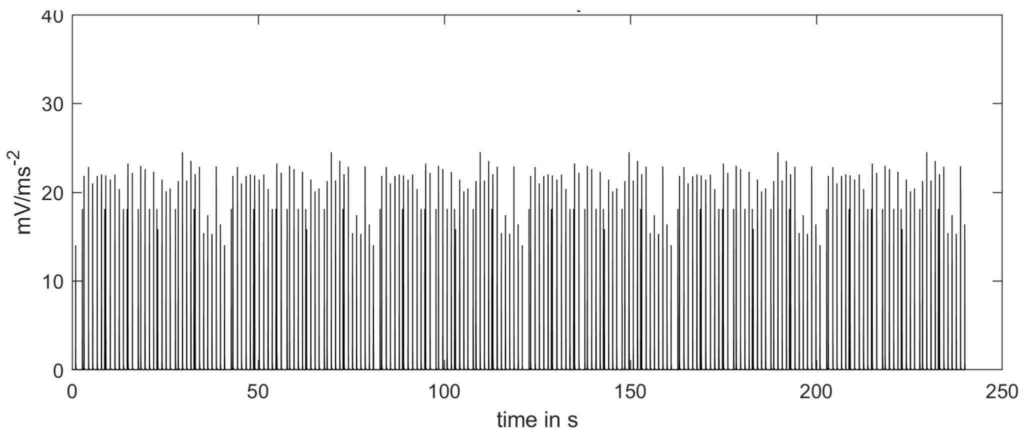

Figure 6.18: Measurement 1: velocity amplitude over time of hammer input example

6.2 Measurement 2

The second measurement also took place in a three-story building still under construction. The building was modular in the sense that the rooms where prefabricated as blocks and assembled on site.

One wall-floor X-junction was measured between level 2 and 3. The setup and method was the same as measurement 1.

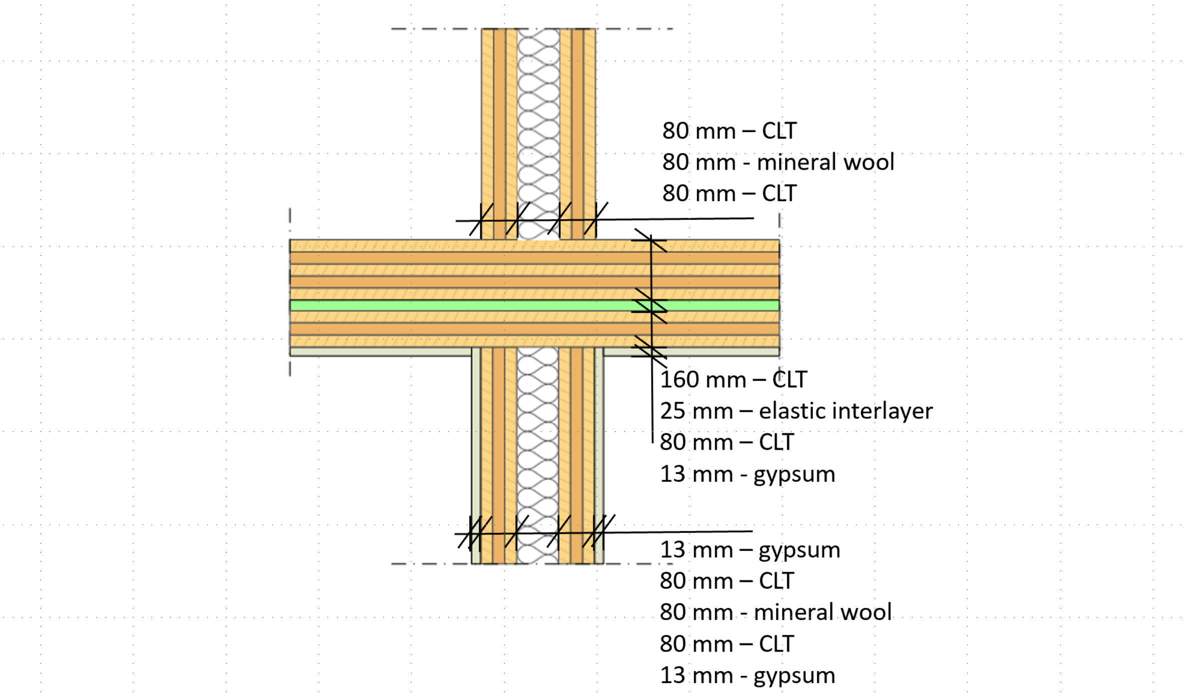

Figure 6.19: Measurement 2: Measured junction dimensions

Figure 6.20: Measurement 2: Wall-floor junction

Figure 6.21: Measurement 2: Internal wall

Figure 6.22: Measurement 2: Ceiling

7

Measured results

The three junctions that were measured are presented below. Figure 7.1 is two external walls separated by a floor on the sixth level.

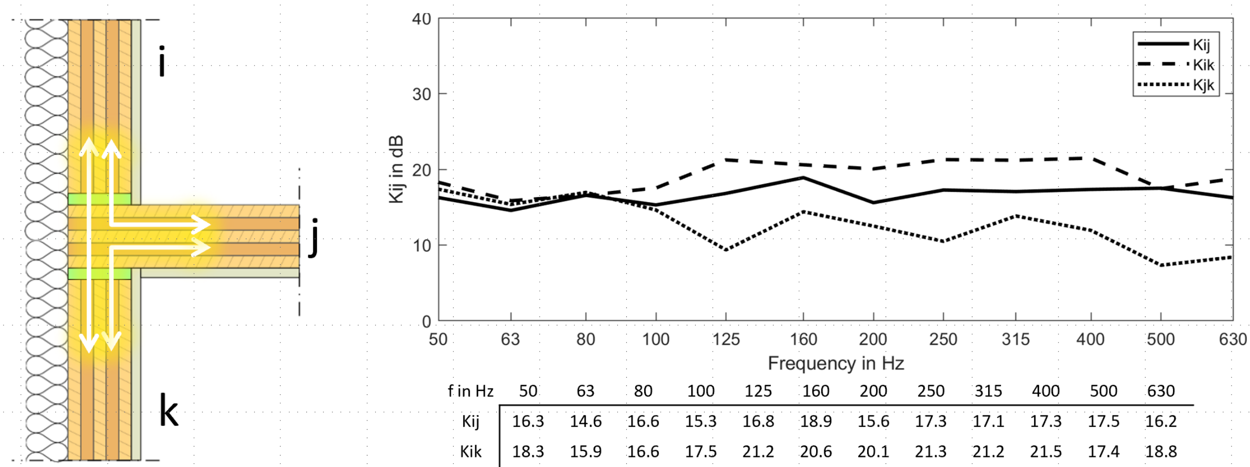

f in Hz	50	63	80	100	125	160	200	250	315	400	500	630
Kij	16.3	14.6	16.6	15.3	16.8	18.9	15.6	17.3	17.1	17.3	17.5	16.2
Kik	18.3	15.9	16.6	17.5	21.2	20.6	20.1	21.3	21.2	21.5	17.4	18.8
Kjk	17.4	15.4	17.0	14.6	9.4	14.4	12.5	10.5	13.8	11.9	7.3	8.4

Figure 7.1: Measurement 1: K_{ij} of external wall level 5 and 6

Figure 7.2 is the junction of internal walls and floor separating the fifth and sixth level.

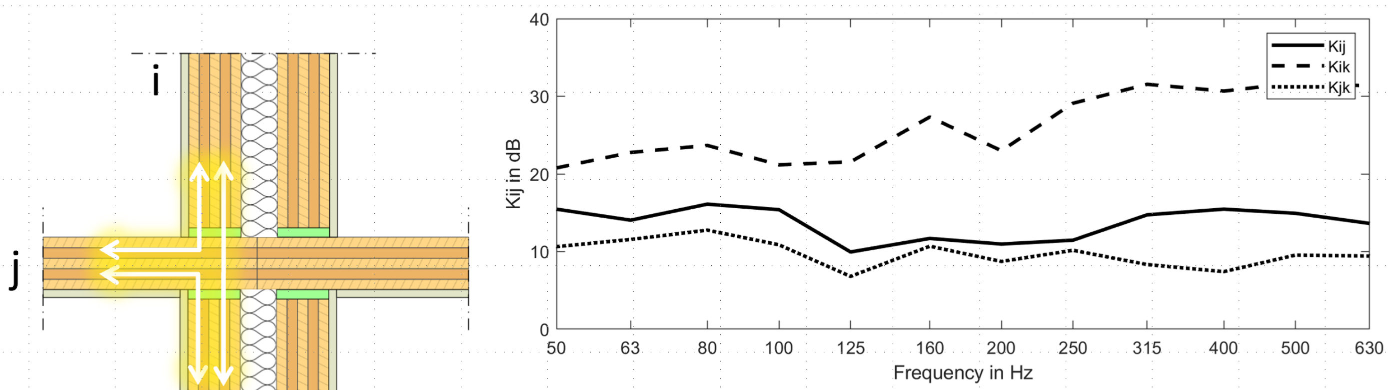

f in Hz	50	63	80	100	125	160	200	250	315	400	500	630
Kij	15.5	14.0	16.1	15.4	9.9	11.7	11.0	11.5	14.7	15.5	14.9	13.6
Kik	20.8	22.8	23.7	21.2	21.6	27.3	23.0	29.1	31.5	30.7	31.7	31.3
Kjk	10.6	11.6	12.8	10.9	6.8	10.7	8.7	10.1	8.3	5.4	9.5	9.4

Figure 7.2: Measurement 1: K_{ij} of internal wall level 5 and 6

The final junction of measurement 1 (Figure 7.3) is the internal walls-floor junction separating the fourth and fifth level.

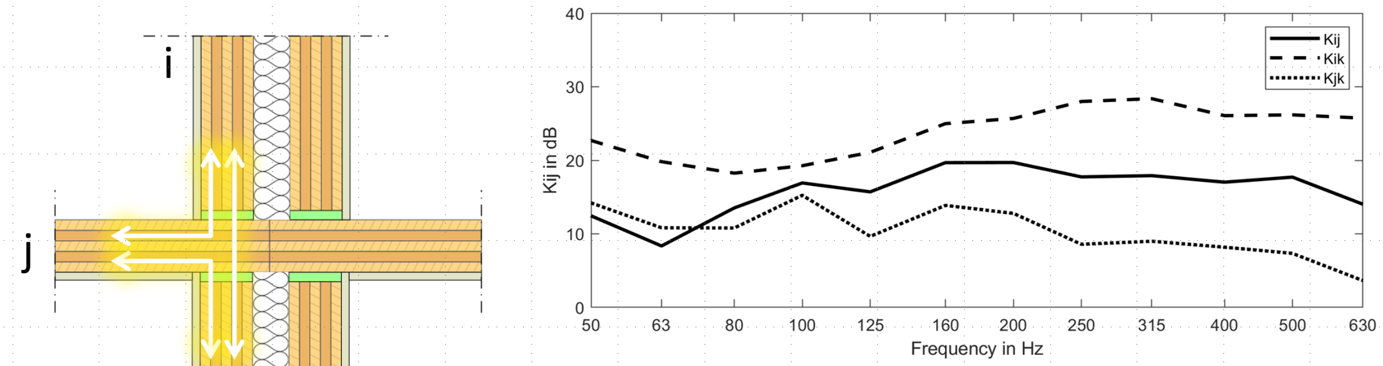

f in Hz	50	63	80	100	125	160	200	250	315	400	500	630
Kij	12.5	8.4	13.5	16.9	15.7	19.7	19.7	17.7	17.9	17.0	17.7	14.0
Kik	22.7	19.8	18.3	19.3	21.1	25.0	25.7	28.0	28.4	26.1	26.2	25.7
Kjk	14.2	10.8	10.8	15.2	9.7	13.9	12.8	8.6	9.0	8.2	7.3	3.6

Figure 7.3: Measurement 1: K_{ij} of internal wall level 4 and 5

Figure 7.4 details the results from the measured wall-floor junction between level 2 and 3 from measurement 2.

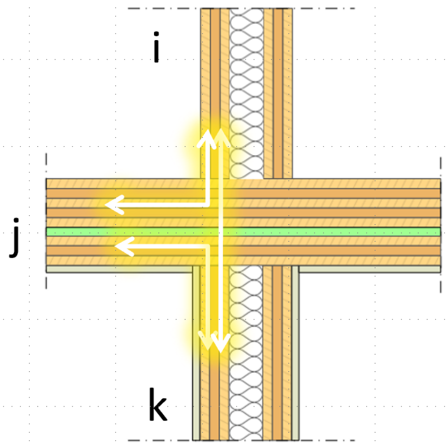

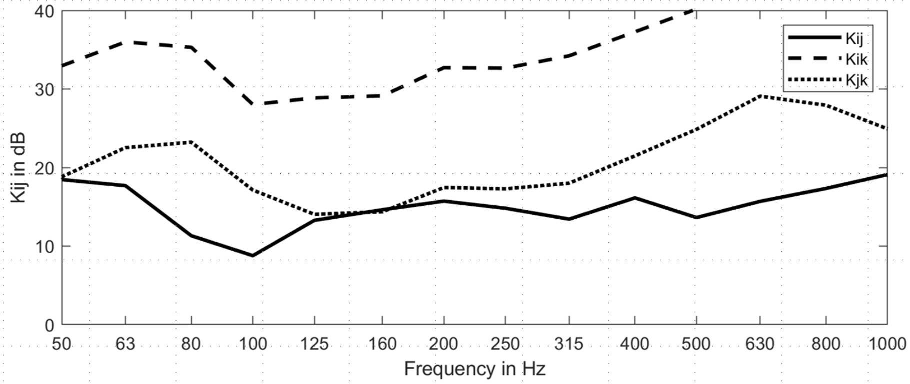

f in Hz	50	63	80	100	125	160	200	250	315	400	500	630	800	1000
Kij	19.3	18.5	12.2	9.6	14.1	15.5	16.6	15.7	14.3	17.0	14.5	16.5	18.2	20.0
Kik	33.8	36.8	36.1	28.9	29.7	30.0	33.6	33.5	35.1	38.1	41.0	44.4	44.5	44.1
Kjk	20.1	23.8	24.5	18.4	15.3	15.6	18.7	18.5	19.3	22.7	26.1	30.3	29.2	26.2

Figure 7.4: Measurement 2: K_{ij} of internal wall-floor junction of level 2 and 3

8

Discussion

8.1 Measurement uncertainty

As mentioned in section 6.1 the power input of the impact hammer was not recorded during the measurements due to limitations of the measurement equipment. This deviation from the standard required more samples. In measurement 1 each signal is a result of an averaging of 240 impulses. The number of impulses for each signal in measurement 2 is 320. In Figure 8.1 and 8.2 the standard error has been calculated and plotted as a 97.5% confidence interval for each element excited, as recorded by accelerometers mounted on one element per measurement. The biggest uncertainty can be found in frequency band 315 Hz in measurement 2 when excitation occurs in the same element as the accelerometers are mounted. At that data point there is a 97.5% that the true value is within 2.9 dB above or below the measured value. It makes sense that the biggest uncertainty occurs when exciting the same element that the accelerometers are mounted on, since there is a higher possibility that the measurement is not taking place in the reverberant field.

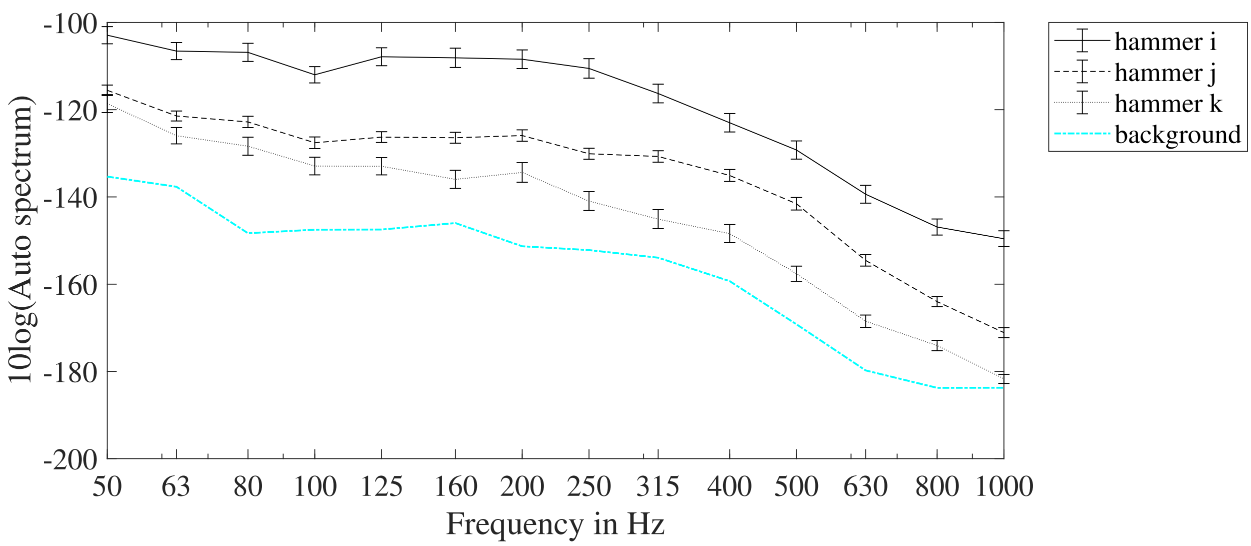

Figure 8.1: Measurement 1: Confidence interval (97.5%) of signals recorded by accelerometer mounted on element i

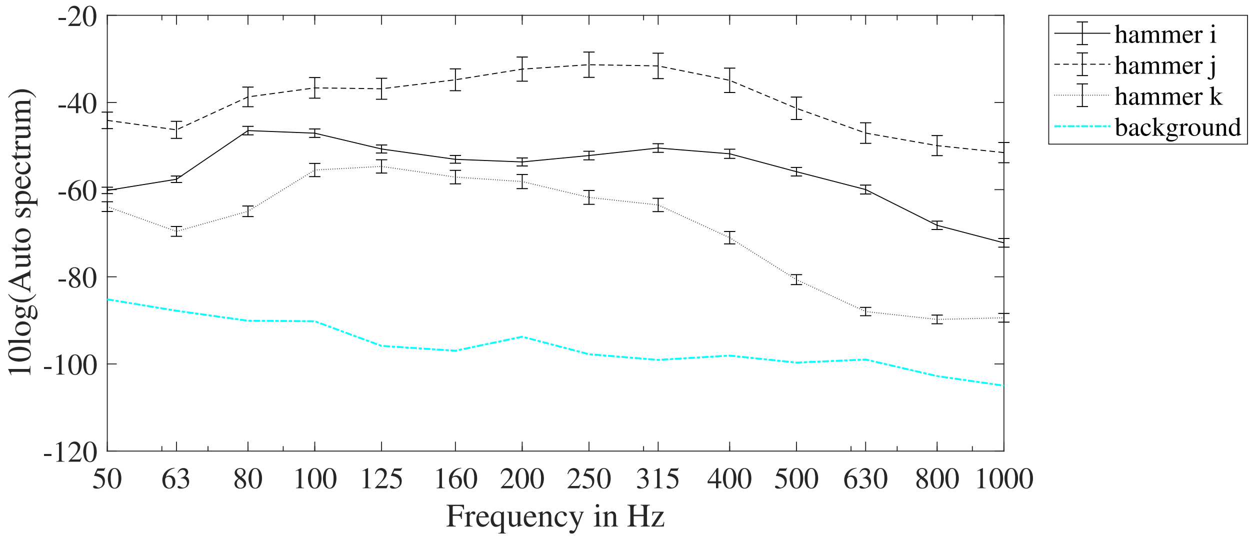

Figure 8.2: Measurement 2: Confidence interval (97.5%) of signals recorded by accelerometer mounted on element j

8.2 Load

How the behavior of the junction change with increasing load becomes visible when comparing the same junction at different levels in the building. Figure 8.3 shows all three measured junction paths of the internal wall-floor X-junction on the highest levels of the building (5 and 6) and the levels below (4 and 5). The straight wall to wall path of the lower junction performs worse in all but one frequency bands (200 Hz). The perpendicular upper wall-floor path of the lower junction performs worse under 100 Hz and the same or better in the frequency band of and above 100 Hz. The perpendicular lower wall-floor path of the lower junction is rather similar to the upper junction but performs slightly better in the frequency bands 50,100,125,160,200,315,400 Hz and slightly worse in 63,80,250,500,630 Hz. This is the first straight path under load comparison presented in the thesis, since both examples in section 8.2 where of perpendicular paths.

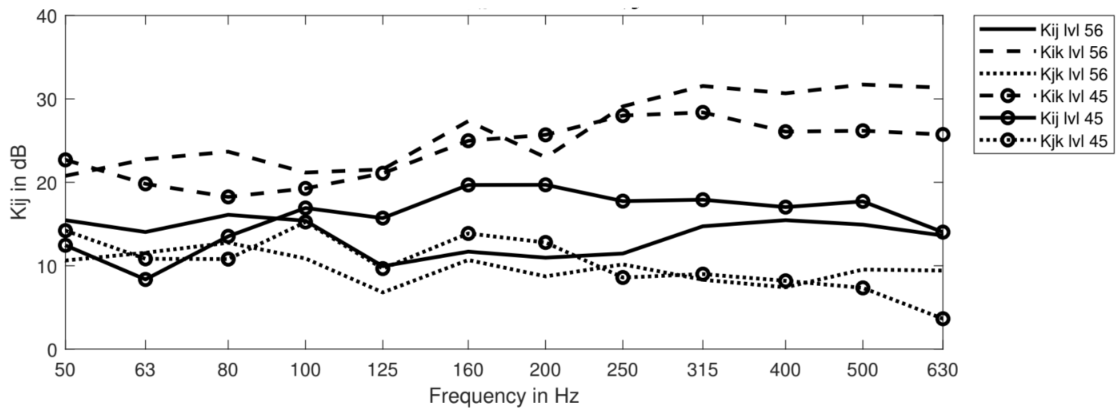

Figure 8.3: Measurement 1: K_{ij} of internal wall junctions

8.3 Internal and external wall junctions

In Figure 8.4 the internal wall-floor junction between level 5 and 6 is compared to an external junction of the same floor. The external wall is a T-junction while the internal wall is a X-junction shared with another wall element separated by 75 mm mineral wool (Figure 6.8). The straight wall to wall path of the external junction performs worse than that of the internal. Both perpendicular paths of the external junction perform slightly better or about the same as the internal junction. Overall there is less difference between the three junction paths in the external junction than in the internal.

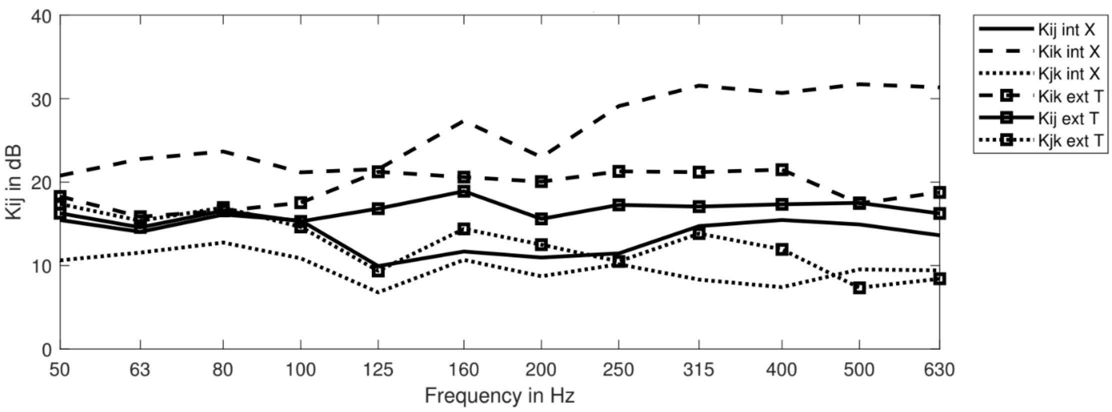

Figure 8.4: Measurement 1: K_{ij} of internal and external wall junctions

8.4 Junction composition

The composition of a junction will of course impact the vibration transmission behavior. In Figure 8.5 the junctions of measurement 1 and 2 are compared. The junction of measurement 1 is the internal wall-floor junction on the highest floor level. The straight wall-wall path and the perpendicular lower wall-floor path are greatly improved by the modular approach utilized in measurement 2.

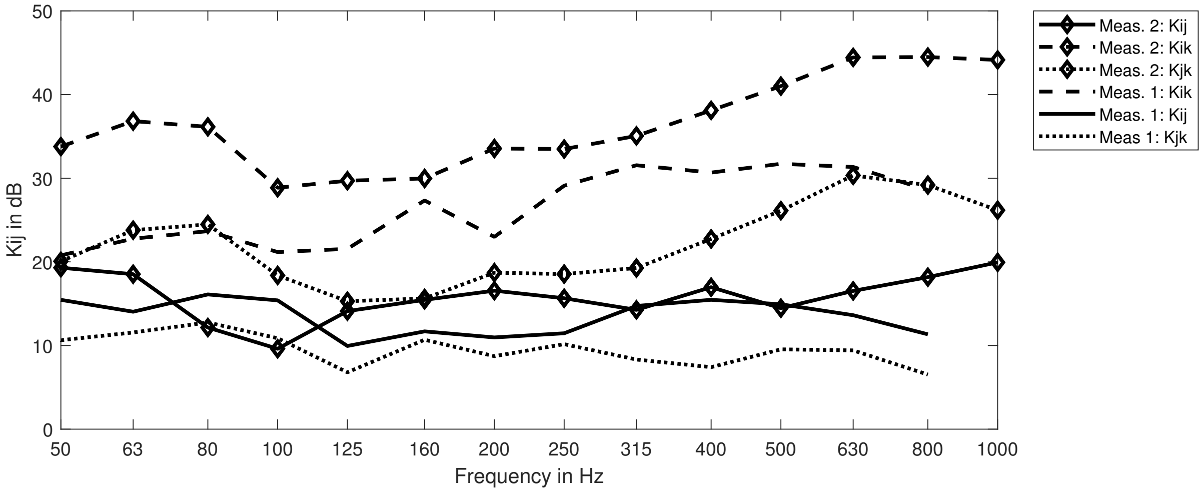

Figure 8.5: K_{ij} junctions in measurement 1 and 2

8.5 Lab vs in-situ measurements

In a comparison between of the measured internal junction on the highest levels and a similar x-junction measured in lab for the Flanksound project (Rothoblaas, 2018), Figure 8.7 is the result. It is not a perfect comparison with the main difference being that the lab specimen has thinner vertical elements and a thicker floor element. The lab specimen consists of 100mm-3ply wall elements and the floor is a 160mm-5ply element. The floor is screwed to the bottom wall with 300mm steps, and the top wall is connected to the floor via angle brackets with 800mm steps. There is a resilient interlayer at both connections between wall and floor (Figure 8.6).

The straight wall to wall path of the lab specimen performs worse than the in-situ measured junction. This can possibly be explained by the previously stated fact that the lab elements are thinner and therefore vibrate more easily, but on the other hand the difference in thickness between the walls and the floor should cause an impedance change reflecting back much of the energy instead of transmitting. The two perpendicular paths of the lab specimen perform better than the in-situ measured junction in all but one frequency band respectively.

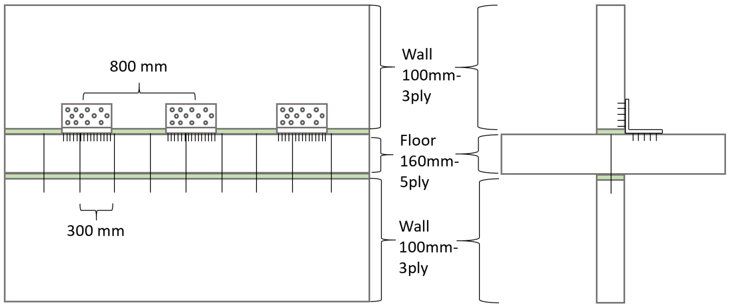

Figure 8.6: Lab specimen, Rothoblaas T-junction

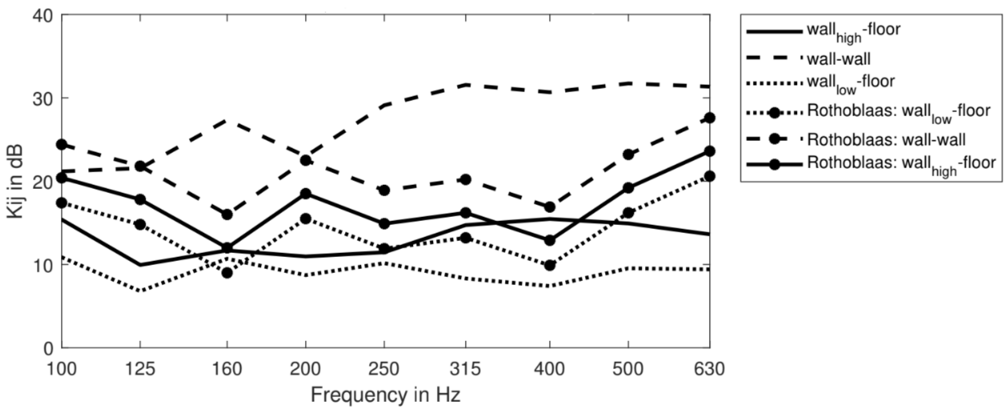

Figure 8.7: K_{ij} of internal wall (measurement 1) compared to similar lab measured specimen

Comparing the in-situ measured external wall junction with a similar T-junction from the Flanksound project produce the following result (Figure 8.9). The lab specimen consists of a two 100mm-3ply wall elements and the floor is a 160mm-5ply element. The floor is screwed to the bottom wall with 300mm steps, and the top wall is connected to the floor via angle brackets with 800mm steps. There is a resilient interlayer at both connections between wall and floor (Figure 8.8).

The junction path that sticks out is one of the perpendicular paths in the lab specimen. This big difference between the vibration transmission from floor to the upper or lower wall is not clearly seen in the in-situ measurement. The two other junction paths are relatively similar between the lab and in-situ measured junctions.

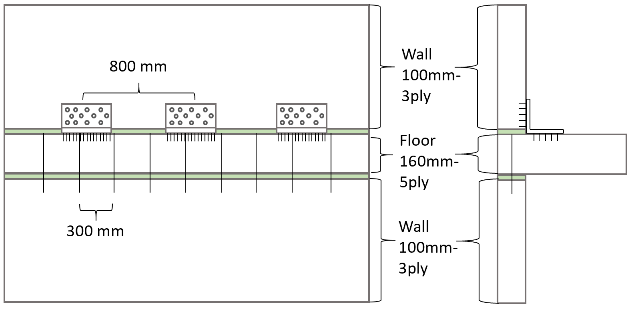

Figure 8.8: Lab specimen, Rothoblaas T-junction

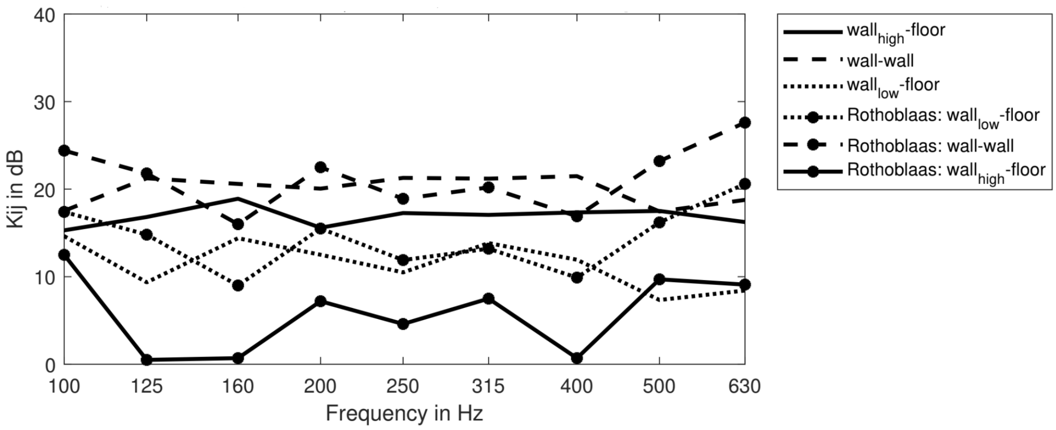

Figure 8.9: K_{ij} of external wall (measurement 1) compared to similar lab measured specimen

Elastic interlayers are common in CLT-constructions. It is rather expensive and at the same time the benefits are not fully understood. The behavior is well studied in lab environment. In those experiments the main influence of it's effectiveness is whether the interlayer is shortcut by screws or not and the resonances of the mass-spring system created by the CLT element and the elastic interlayer. In a realized building however there are other factors that play a role in the final junction performance

- The interlayer is under an increasing load depending on the floor level and the height of the building.
- The assembly is not necessarily as precisely assembled as in a lab environment
- There are many more resonant subsystems present which share the energy
- Boundary conditions are not necessarily the same as the ones studied in a lab environment.

These factors can either increase or decrease the effectiveness of the elastic interlayer. The issue of increased loads are still somewhat unanswered. The perpendicular paths seem to benefit to some extent by being exposed to an external load on the junction. This may be because it hinders the resonance frequencies of the mentioned mass-spring system, which does not appear to be prominent in any of the in-situ measurements. As that load increases it seems to stop being beneficial and the effectiveness of the elastic interlayer decrease. The straight paths of a junction does even worse under load than the perpendicular paths as seen both in the measured in-field measurement and the measurements discussed in section 8.2. The mass-spring effects may also be mitigated in-field by the fact that the boundary conditions are different since the element is baffled at all edges by surrounding structure.

8.6 Standard estimations

A comparison of the measurements in section 7 and the K_{ij} estimation, provided by ISO 12354-1 Annex E, is presented in Figures 8.10 and 8.11. K_{13} is the straight path which corresponds to the measured K_{ik}, and K_{12} is the perpendicular path which corresponds to the measured K_{ij} and K_{jk}. The estimation is calculated for a "wall junction with flexible interlayers" as detailed in section 4. The estimations does not fit well with the in-field measurements, especially in low frequencies where the vibration reduction index is underestimated.

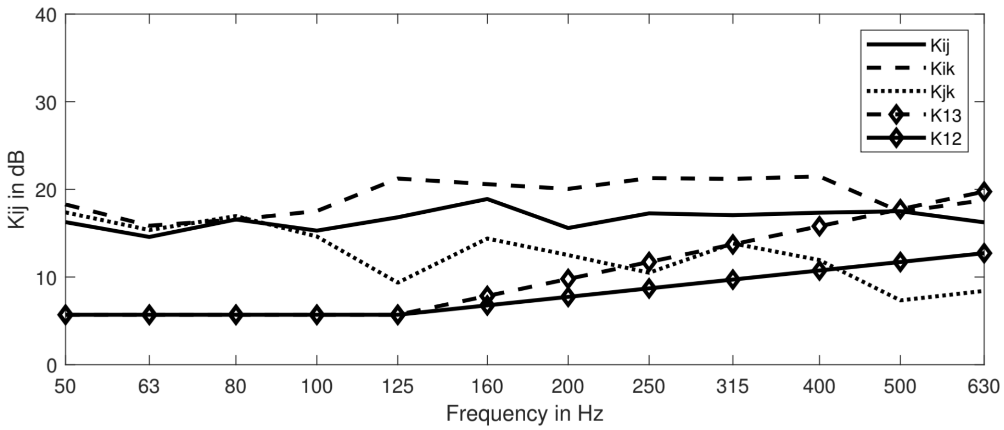

Figure 8.10: Vibration reduction index of external wall T-junction (measurement 1) compared to estimation in ISO 12354-1 (Marker: Diamond)

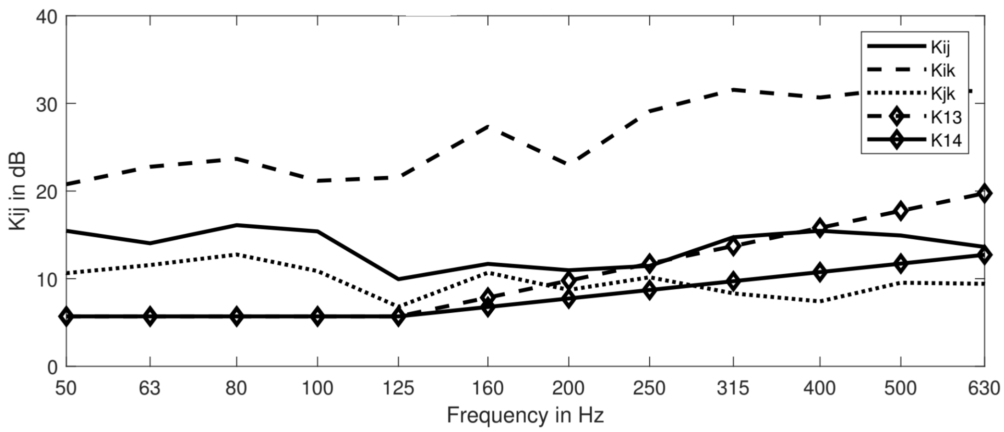

Figure 8.11: Vibration reduction index of internal wall X-junction (measurement 1) compared to estimation in ISO 12354-1 (Marker: Diamond)

8.7 Element composition

The choice of CLT element is going to play a big role in the resulting sound transmission in a building. The more orthotropic the material is the wider the radiation peak as seen in section 3.3. It is the reason why flanking transmission in the mid-frequency range is so important. If CLT elements are chosen that are more isotropic, then the radiation should also become more easy to control.

9

Conclusion

This thesis has examined the structure-borne vibrations transmitted through cross laminated timber junctions. The main method to reduce flanking transmission through these connection points in a building is to create an impedance change within the junction. Utilizing different thicknesses of CLT element connected to any particular junction will reduce vibration transmission (section 3.7). Depending on the CLT element chosen, the material properties can vary significantly (section 3.1). This can, much like the change in geometry, also cause a change in impedance, which is favorable in the case of junction transmission. On the other hand, the more orthotropic elements create a wider radiation efficiency peak (section 3.3) which might bypass the possible gains made in the junction transmission.

Floors and ceilings can be treated with floating layers to mitigate noise transmission. However, the impact of first order flanking on the total sound transmission between two rooms completely depend on the structure-borne vibration transmission through the wall to wall junction, and whether additional layers are present on connected elements, such as one or two layers of gypsum. The encouraging fact is that the wall to wall junction path consistently performs better than the perpendicular paths. The less encouraging fact is that the wall to wall junction path performed worse when going down one level (i.e. increasing the load) in the in-field measurement performed in this thesis (section 8.2). With increasing load the effectiveness of isolation through the means of elastic interlayers will be limited. The taller the building becomes, the harder it is going to be to treat this specific path without excessive or innovative solutions such as treating the walls acoustically or utilizing blocking mass or rolling connections in the junction (section 3.4).

Annex E of the standard ISO 12354-1 is not yet well suited for estimation of vibration reduction indexes with regards to CLT-constructions (section 8.6), as it tends to underestimate the real life performance. Finite element modeling shows potential to estimate the structure-borne vibration transmission in low to mid frequencies (section 5).

10
Further studies

Future work could contain the following tasks.

1. Measure the vibration reduction index in realized buildings with a focus on the difference between high and low floor levels.
2. Continue finite element modeling of junctions, with focus on if the influence of connections and elastic interlayers can be sufficiently estimated by comparing the FE-analysis result to lab measurement.
3. Make detailed measurements in lab with the aim to determine damping, modal response and radiation efficiency of different CLT elements.
4. Test alternative isolators in junctions that can withstand high static vertical loads.

Bibliography

Rune Abrahamsen. World's tallest timber building – 14 storeys in bergen. 2015.

Ulf Aronsson. Stora enso investerar i kl-trä i gruvön, 2017a. URL `https://www.atl.nu/skog/stora-enso-investerar-i-kl-tra-i-gruvon/`.

Ulf Aronsson. Stort sug efter kl-trä, 2017b. URL `https://www.atl.nu/skog/stort-sug-efter-kl-tra/`.

Tobias Augustsson. *Evaluating SEA modelling of lightweight building elements containing cross laminated timber*. PhD thesis, Master's thesis, Chalmers University of Technology, Division of Applied . . . , 2016.

David Barber. Tall timber buildings: What's next in fire safety ? *Fire Technology*, 51(6):1279–1284, Nov 2015. ISSN 1572-8099. doi: 10.1007/s10694-015-0497-7. URL `https://doi.org/10.1007/s10694-015-0497-7`.

Delphine Bard, Peter Davidsson, and Per-Anders Wernberg. Sound and vibrations investigations in a multi-family wooden frame building. In *Proceedings of the 20th International Congress on Acoustics. Sydney, August*, pages 23–27, 2010.

Reinhard Brandner, Georg Flatscher, Andreas Ringhofer, Gerhard Schickhofer, and Alexandra Thiel. Cross laminated timber (clt): overview and development. *European Journal of Wood and Wood Products*, 74(3):331–351, 2016.

L Cremer, M Heckl, and EE Ungar. Structure-borne sound. 1988.

Ch Crispin, C Mertens, M Blasco, B Ingelaere, M Van Damme, and D Wuyts. The vibration reduction index kij: laboratory measurements versus predictions en 12354-1 (2000). In *INTER-NOISE and NOISE-CON Congress and Conference Proceedings*, volume 2004, pages 2071–2077. Institute of Noise Control Engineering, 2004.

Christian Dagenais, Robert H White, and Kuma Sumathipala. Clt handbook (us edition): Chapter 8-fire performance of cross-laminated timber elements, 2013.

HJ Darby, Abbas Ali Elmualim, and Fergal Kelly. A case study to investigate the life cycle carbon emissions and carbon storage capacity of a cross laminated timber, multi-storey residential building. In *Proceedings of the Sustainable Building Conference, Munich, Germany*, pages 10–12, 2013.

Franz Dolezal, Thomas Bednar, and Martin Teibinger. Flankenübertragung bei massivholzkonstruktionen–teil 2: Einfluss von befestigungsmitteln auf die verbesserung durch den einbau elastischer zwischenschichten. *Bauphysik*, 30(5): 314–319, 2008.

D Fell. Wood and human health, 2013.

Vladimir Gintoff. Construction of the world's tallest timber tower is underway in vancouver, 2016. URL `https://www.archdaily.com/787673/construction-of-the-worlds-tallest-timber-tower-is-underway-in-vancouver`.

Wood Handbook. Wood handbook-wood as an engineering material. *General Technical Report FPL-GTR-190, Department of Agriculture, Forest Service, Forest Products Laboratory: USA*, 2010.

Viktor Hansson and Olle Hervén. Sverige bygger högt i trä. 2011. Student Paper.

Carl Hopkins. *Sound insulation*. Elsevier, 2007.

EN ISO. 10848-1: 2017. *Acoustics - Laboratory and field measurement of flanking transmission for airborne, impact and building service equipment sound between adjoining rooms-Part 1: Frame document*, 1, 2000.

EN ISO. 12354-1: 2000. *Building acoustics–Estimation of acoustic performance of buildings from the performance of elements–Part 1: Airborne sound insulation between rooms*, 2, 2017.

Yiwei Kou, Bilong Liu, and Jing Tian. Radiation efficiency of damped plates. *The Journal of the Acoustical Society of America*, 137(2):1032–1035, 2015.

Wolfgang Kropp. Propagation and radiation of structure borne sound. 2015.

Francis Godfrey Leppington, Edward Granville Broadbent, and KH Heron. The acoustic radiation efficiency of rectangular panels. *Proc. R. Soc. Lond. A*, 382 (1783):245–271, 1982.

Sten Ljunggren. Ljudisolering i trähus: en handbok för konstruktörer. akulite rapport 1, 2011.

Martinsons. Konstruktionsfakta kl-tra. URL `https://www.martinsons.se/wp-content/uploads/2019/02/KL-tra_konstruktionsfakta_tab_webb.pdf`.

Birgit Östman and Bo Källsner. National building regulations in relation to multistorey wooden buildings in europe. *SP Trätek and Växjö University, Sweden*, 2011.

Rothoblaas. Soundproofing solutions. 2018.

Andrea Santoni, Patrizio Fausti, Stefan Schoenwald, and Hans-Martin Tröbs. Sound radiation efficiency measurements on cross-laminated timber plates. In *INTER-NOISE and NOISE-CON Congress and Conference Proceedings*, volume 253, pages 5979–5989. Institute of Noise Control Engineering, 2016a.

Andrea Santoni, Stefan Schoenwald, Bart Van Damme, Hans-Martin Tröbs, and Patrizio Fausti. Average sound radiation model for orthotropic cross laminated timber plates. *Proc EuroRegio*, pages 13–15, 2016b.

Aline Timpte. Vibration reduction indices of cross laminated timber structures. 2016.

Nikolaos-Georgios Vardaxis. Finite element modeling for cross laminated timber constructions. 2014.